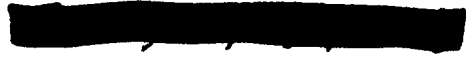


601139

2 of 3



# A Review of Nuclear Explosion Phenomena Pertinent to Protective Construction

H. L. Brode

May 1964

R-425-PR

A REPORT PREPARED FOR  
UNITED STATES AIR FORCE PROJECT RAND

DDC  
RECEIVED  
JUN 15 1964  
RESERV  
IIGA D

20041215104

The RAND Corporation

1700 MAIN ST • SANTA MONICA • CALIFORNIA • 90406

BEST AVAILABLE COPY

This research is sponsored by the United States Air Force under Project RAND—Contract No. AF 49(638)-700—monitored by the Directorate of Development Planning, Deputy Chief of Staff, Research and Development, Hq USAF. Views or conclusions contained in this Report should not be interpreted as representing the official opinion or policy of the United States Air Force.

DDC AVAILABILITY NOTICE

Qualified requesters may obtain copies of this report from the Defense Documentation Center (DDC).

# A Review of Nuclear Explosion Phenomena Pertinent to Protective Construction

*H. L. Brode*

May 1964

R-425-PR

A REPORT PREPARED FOR  
UNITED STATES AIR FORCE PROJECT RAND

---

The **RAND** Corporation

1700 MAIN ST • SANTA MONICA • CALIFORNIA • 90406

Copyright © 1964

THE RAND CORPORATION

## PREFACE

DURING THE 20 YEARS when applications of nuclear weapons have been of national concern, interest in weapons effects has moved closer to the source of the explosion and so toward more and more intensely damaging forces, requiring heavier protection to ensure survival. In the present report the author incorporates some of the growing knowledge about these forces into a summary of close-in effects and a review of the physical phenomena pertinent to protective construction. Although this compilation draws on the results of many studies and on material from many sources, it is in large part based on theoretical calculations of explosion phenomena done at The RAND Corporation.

## SUMMARY

SPECIFICALLY ORIENTED to the design of protection from the effects of nuclear weapons, this report deals with the phenomena of the intense or close-in regions not always adequately covered in such otherwise thorough standard works as Glasstone's *The Effects of Nuclear Weapons*.<sup>(1)</sup> Some features given emphasis are early fireball growth, prompt nuclear radiation near an explosion, cratering and intense ground shock, high-overpressure air blast, hot fireball air and intense thermal exposure, and distribution of debris and after-winds. The intention, however, has been to include information on all aspects of nuclear explosions known to be pertinent to the design of shelters.

## CONTENTS

PREFACE .....	iii
SUMMARY .....	v
FIGURES .....	ix
SECTION	
I. INTRODUCTION .....	1
II. FIREBALL FORMATION .....	3
III. THERMAL RADIATION .....	7
IV. NUCLEAR RADIATION .....	13
V. ELECTROMAGNETIC PULSE .....	20
VI. CRATERING AND DIRECT GROUND SHOCK .....	21
Cratering .....	21
Direct Ground Shock .....	28
VII. AIR BLAST .....	31
Shock Parameters .....	31
Blast Loading on Structures .....	38
Shock Propagation in Tunnels .....	44
VIII. AIR-BLAST-INDUCED GROUND SHOCK .....	51
Superseismic Ground-shock Maxima (at 5-ft Depth) .....	52
Outrunning Ground-shock Maxima (at ~10-ft Depth) .....	53
Attenuation with Depth .....	54
Shock Spectra .....	56
IX. DEBRIS AND FALLOUT .....	59
X. FIRES .....	62
REFERENCES .....	65

## FIGURES

1. Initial Fireball Growth .....	4
2. Fireball Temperature versus Radius at Early Times in the Fireball History (1-MT Surface Burst) .....	5
3. Fireball Density versus Radius at Early Times in the Fireball History (1-MT Surface Burst) .....	5
4. Overpressure versus Range at Early Times in the Shock-wave Growth (1-MT Surface Burst) .....	6
5. Late Fireball Temperature versus Radius (1-MT Surface Burst) .....	8
6. Thermal Radiation Rate .....	9
7. Temperature versus Time at High Peak Overpressures (1-MT Surface Burst) .....	9
8. Transmissivity as a Function of Distance in Units of Visibility .....	11
9. Shock Influence on Prompt Gamma Rays (a Moving Shield) .....	15
10. Half-thickness for Gamma-ray Attenuation .....	17
11. Crater Dimensions versus Depth of Burst (1 KT) .....	22
12. Crater Scaling .....	23
13. Initial Conditions for Surface-burst Cratering Motion .....	24
14. Earth Pressure Contours from Surface Burst ( $t = 0.1$ ms) .....	25
15. Particle Velocities from Surface Burst ( $t = 0.1$ ms) .....	25
16. Earth Pressure Contours from Surface Burst ( $t = 52$ ms) .....	26
17. Particle Velocities from Surface Burst ( $t = 52$ ms) .....	27
18. Earth Pressure Contours from Surface Burst ( $t = 105$ ms) .....	27
19. Particle Velocities from Surface Burst ( $t = 105$ ms) .....	28
20. Peak Stress versus Depth in Hard Rock (beneath Surface or Shallow-buried Bursts) .....	29
21. Peak Stress Contours for 1-MT Hard Rock .....	29
22. Overpressure versus Radius (1-MT Surface Burst) .....	31
23. Shock Radius ( $R_s$ ) and Arrival Time ( $t_s$ ) versus Peak Overpressure for a 1-MT Surface Burst .....	32

24. Approximate Analytic Form for Overpressure versus Time for Nuclear Blast Wave in Terms of Peak Overpressure .....	34
25. Approximate Analytic Form for Dynamic Pressure versus Time for Nuclear Blast Wave in Terms of Peak Overpressure .....	35
26. Form Factors for Overpressures from Nuclear Explosions .....	36
27. Form Factors for Dynamic Pressures from Nuclear Explosions .....	37
28. Shock-wave Peak Pressures (1-MT Surface Burst) .....	38
29. Shock Parameters versus Shock Overpressure .....	39
30. Impulses and Durations for Overpressure and Dynamic Pressure for 1-MT Nuclear Surface Burst versus Peak Overpressure .....	40
31. Shock Configurations (Air Burst) .....	41
32. Reflection Factors for Normal Shocks at Sea Level .....	42
33. Reflection Factors versus Incident Angle and Shock Strength .....	43
34. Average Front-face Pressure versus Time (Closed Rectangular Structure) .....	44
35. Average Pressure on Sides or Top versus Time (Closed Rectangular Structure) ...	45
36. Net Translational Pressure versus Time (Closed Rectangular Structure) .....	45
37. Shock-tube Boundary Layer .....	47
38. Shock-tube Attenuation Data at High Overpressure .....	47
39. Shock-tube Attenuation Data at Low Overpressure .....	48
40. Shock-attenuation Schemes .....	49
41. Water Door .....	50
42. Vertical Accelerations at Shallow Depths .....	52
43. Air-shock-induced Ground Motion Wave Fronts for Peak Overpressures of 10,000, 1000, 300, and 100 psi, and for Seismic Velocities of 2500 ft/sec and 5000 ft/sec	55
44. Geometric Attenuation with Depth .....	57
45. Vertical Shock Spectra .....	58
46. Late Fireball Densities (1-MT Surface Burst) .....	59
47. Late Fireball Turbulence .....	60

## I. INTRODUCTION

LARGE-YIELD WEAPONS create an environment of air and ground shock and of thermal, nuclear, and electromagnetic radiations in intensities that military systems designers have not until recent years been obliged to consider. A clear picture of the nature of a nuclear explosion, reliable estimates of the consequent damage, and some evaluation of what constitutes practical levels of protection are prerequisites for planning the continued operation of essential equipment during and after heavy nuclear attack. Nuclear explosion phenomena are examined in this report with a view toward (1) delineating their influence on the survivability of structures and equipment at very high overpressure levels and (2) providing a general appreciation of the nature of the violent forces with which protective designs must cope.

The following specific areas of nuclear explosion phenomena are discussed (some more completely than others):

- Fireball growth
- Thermal radiation
- Nuclear radiation and shielding
- Electromagnetic radiation
- Cratering and direct ground shock
- Air blast
- Ground shock (air-blast-induced)
- Cloud rise, fallout, debris
- Fires

Although the effects of these phenomena are distinct and separately identifiable, the physical processes responsible for their generation are thoroughly interdependent.

The train of events in a nuclear explosion begins with the nuclear reactions and their radiations, but both the prompt radiation doses and the subsequent fallout activity are influenced greatly by the dynamics of the subsequent explosion. The shocked air and its expansion dictates the nature of the thermal radiation. At the same time, the cratering and associated

throwout interfere with the thermal phenomena. The rising cloud carries aloft debris that constitutes the subsequent fallout and is influenced by the earlier thermal radiation and by the throwout and cratered material, as well as by the air motions generated by the blast. Nearly all these effects, in turn, influence to some extent the blast itself.

## II. FIREBALL FORMATION

IN THE EXPLOSION of a 1-megaton (MT) bomb, energy equivalent to  $10^{15}$  calories (cal) is released in a time much less than a millionth of a second and in a mass of a very few tons. Such high-energy density leads to temperatures of millions of degrees and leaves much of the energy in the form of radiation. This radiation quite quickly diffuses into the air. The radiation from the bomb materials at such high temperatures is mostly in the form of ultraviolet and X rays; and "light" from these high frequencies, unlike ordinary visible light, does not travel great distances in air. Rather, it is absorbed in the air immediately around the bomb, causing that air to be heated to temperatures in the neighborhood of  $1,000,000^{\circ}\text{C}$ . But air at  $1,000,000^{\circ}\text{C}$  becomes quite transparent, even to X rays and ultraviolet light, so that *subsequent* radiation from the bomb can traverse this region of hot air more freely and can be absorbed only when it reaches the outer cold air. By such a process, then, this initial region of hot air grows rapidly as energy pours out of the bomb and is absorbed in the surrounding cold air. The cold air is so opaque to soft X rays that a rather sharp, fast-moving front is maintained between the cold air outside and the hot air inside (Fig. 1).

The initial radiative growth of this high-temperature sphere takes place before hydrodynamic shocks can develop. But as the energy expands by this radiation diffusion process into larger and larger volumes of air, its temperature begins to drop and the speed of the expansion decreases, until at about  $800,000^{\circ}\text{C}$  the rate is comparable to a shock speed at the same temperature. After that, an extremely strong spherical shock front develops and races onward at an extremely high speed. For a 1-MT surface burst, this transition should occur at a radius of about 170 ft from the bomb. The extremely strong shock, driven by the high pressures in this hot sphere, begins to compress the air some tenfold above normal air density and to force it outward close behind the shock front. Since the shock is expanding into continuously larger volumes of air, its strength, and consequently its ability to heat the air it engulfs, decreases rapidly with increasing shock radius. Although the shock-heated air is initially at temperatures well below the interior temperatures, it is hot enough to be intensely

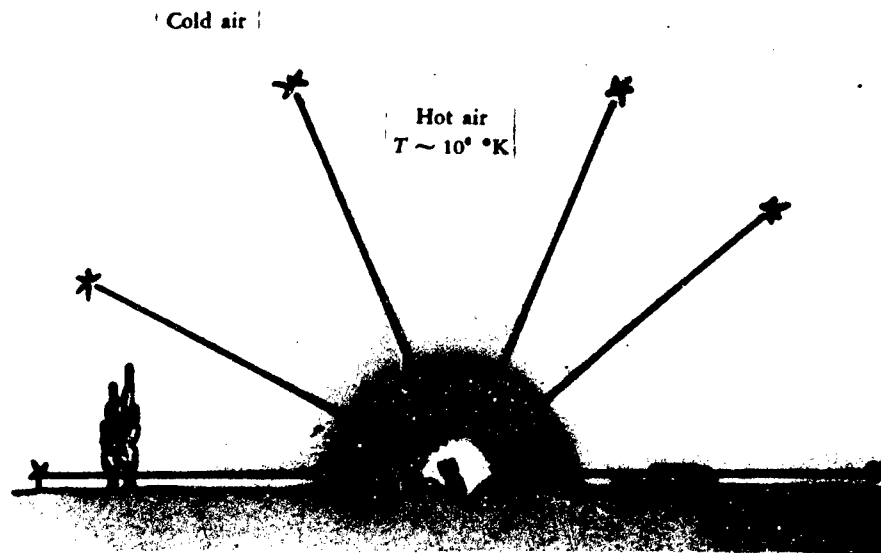


FIG. 1—Initial Fireball Growth

luminous (with intensity many times that of the sun). This shock front is the source of the early thermal radiation. As the shock decreases in strength, its luminosity decreases so rapidly that the total radiation from the fireball also decreases, in spite of the increasing area of the expanding shock front.

Figure 2 illustrates the early temperature history of such a blast wave, showing the temperature in degrees on the Kelvin scale (the absolute centigrade scale) for a 1-MT surface burst. The earliest curve—0.075 millisecond (ms)—is characteristic of the nearly isothermal fireball formed by the radiation diffusion. At later times, the shocked air beyond the isothermal sphere (which itself is expanding and cooling) shows a region of lower temperature. As the shock decreases in strength, it heats the air less, so that the air behind the shock is hotter than that just at the shock, and a steep increasing gradient in temperature exists from the shock front back to the nearly uniform hot interior.

Since the radiation diffusion growth is initially too fast to induce appreciable motions in air, the air is left at essentially normal air density, while its temperature and pressure are raised to values on the order of 1,000,000°C and 1,000,000 pounds per square inch (psi). As the radiation wave slows in its growth and the high pressures begin to build a strong shock, the air in the hot interior begins to expand to lower densities, while the shock that forms at the outer radius compresses the air there to many times normal air density ( $\rho_0 = 1.293 \times 10^{-3}$  grams per cubic centimeter, or  $\text{g/cm}^3$ ). (See Fig. 3.) The interior of the fireball is rapidly

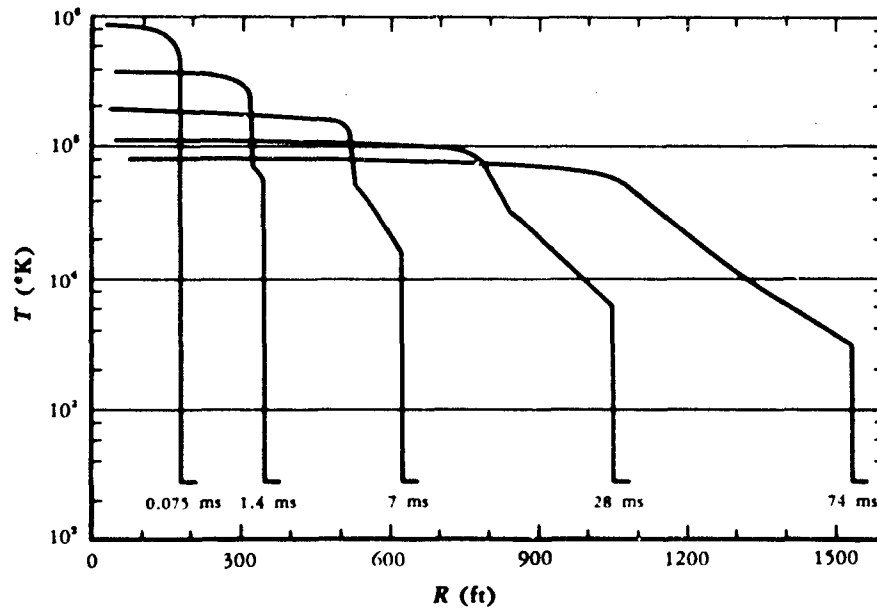


FIG. 2—Fireball Temperature versus Radius at Early Times in the Fireball History (1-MT Surface Burst)

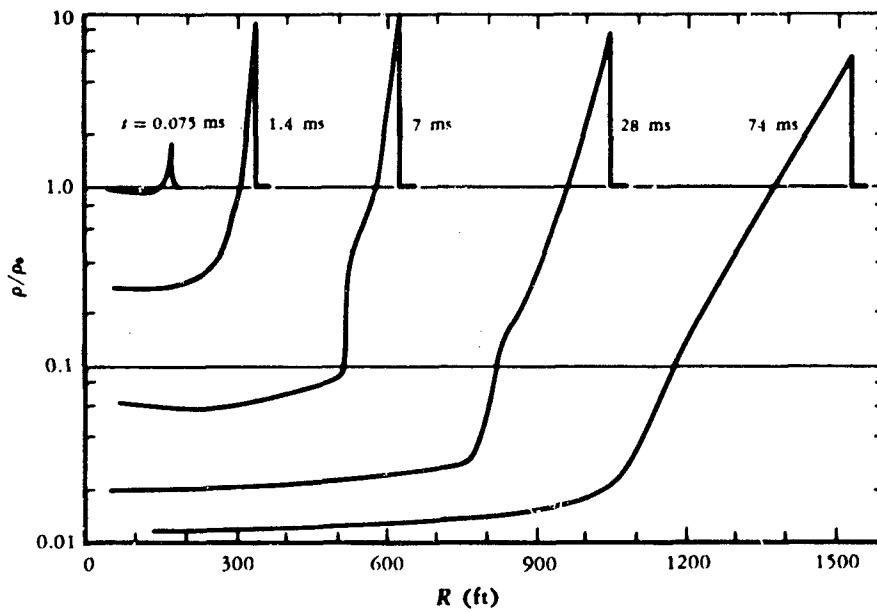


FIG. 3—Fireball Density versus Radius at Early Times in the Fireball History (1-MT Surface Burst)

evacuated, so that by the time the shock has decreased to a peak pressure of 1000 psi ( $\sim 74$  ms at 1500 ft for 1 MT), the interior density is about one-hundredth of normal air density—a fairly good vacuum!

The pressure profiles at these early fireball times are shown in Fig. 4. The earliest air overpressures are indeed on the order of 1,000,000 psi, but they rapidly drop as the fireball grows, so that a peak overpressure of 100,000 psi occurs at about 350 ft (for 1 MT) and an overpressure of 10,000 psi at about twice that distance.

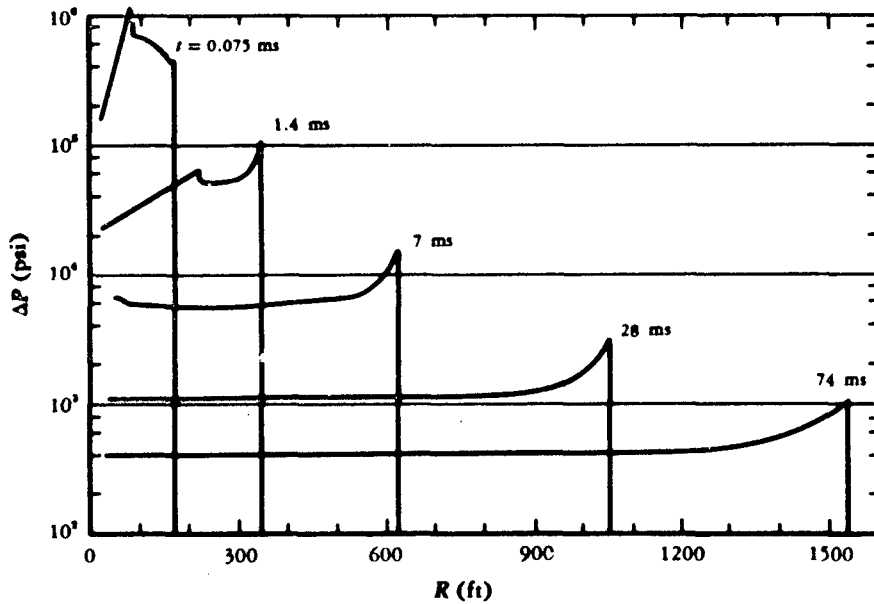


FIG. 4—Overpressure versus Range at Early Times in the Shock-wave Growth (1-MT Surface Burst)

### III. THERMAL RADIATION

FIGURE 5 shows temperature profiles at late fireball times (as indicated) for the same 1-MT surface burst. As was mentioned, most of the earliest light from the bomb cannot travel far in air, but, as a shock develops and the surface of the fireball becomes a sharp shock front, this surface begins to radiate strongly in the visible spectrum at an intensity characteristic of a black body at the shock temperature. At times earlier than those illustrated here, only a fraction of the black-body rate (which is proportional to the fourth power of the temperature) is in the visible spectrum; and only that fraction which is in wave lengths in the visible or infrared spectrum can travel to great distances. The power or rate of thermal radiation at the earlier times can be expressed as proportional to the surface area of the nearly hemispherical fireball ( $2\pi R_s^2$ ) and to the specific black-body radiation rate at the shock temperature ( $\sigma T_s^4$ ), but modified by a factor  $f(T_s)$  representing that fraction of the spectrum which can pass through cold air:

$$P = 2\pi R_s^2 \sigma T_s^4 f(T_s).$$

At times as late as those shown in Fig. 5, the shock front itself is becoming so cool that it is no longer strongly luminous, and the hotter air behind begins to shine through. The hot interior is still expanding, and its radiation intensity is increasing rapidly with the increased effective temperature that can be seen from outside the fireball (i.e., as the outer air becomes more transparent). As a consequence, the thermal power rises rather sharply at this time. As the rate of radiation increases, it becomes a significant heat loss to the fireball and depletes the store of energy in the hot interior. This loss drops the inner temperatures; the thermal power again decreases. The subsequent depletion and cooling rates become less rapid as the temperature drops, so that the thermal intensity trails off over a period of 10 sec or more.

This sequence of optical-hydrodynamic events results first in a fast maximum in the thermal radiation, followed by a minimum at about  $\frac{1}{10}$  sec, and then by a second maximum at about 1 sec. Since the time duration of the first maximum is short and the size of the fireball is small, less than half of 1 per cent of the bomb's energy is radiated before the first

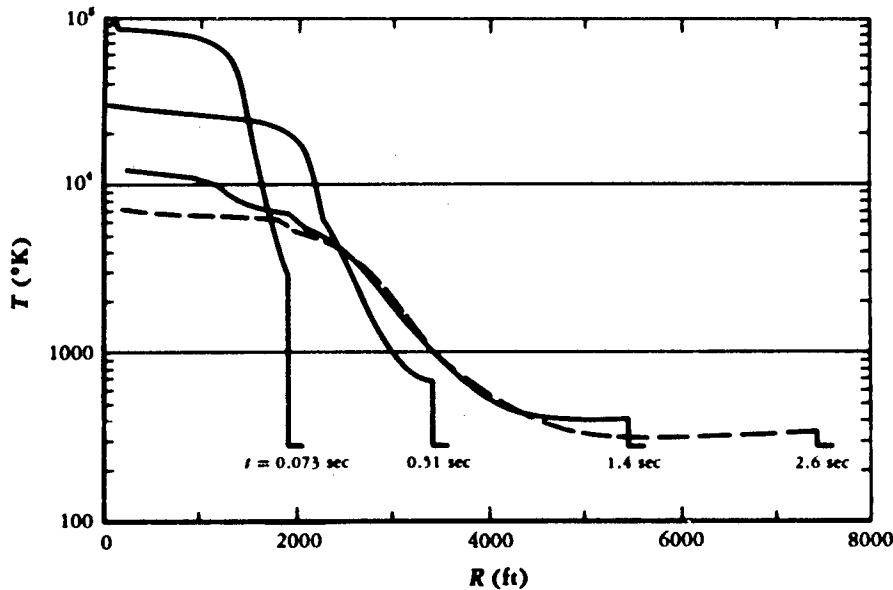


FIG. 5—Late Fireball Temperature versus Radius  
(1-MT Surface Burst)

minimum in the power pulse is reached. The second pulse is longer and radiates from a larger effective surface, and it emits nearly one-third of the total energy of the bomb. The main pulse of thermal radiation reaches a maximum in about 1 sec (for the 1-MT case) and, as mentioned, lasts about 10 sec (Fig. 6).

At very close-in locations the thermal phenomenon may be characterized as an intensely hot "bath" of fireball gases rather than as light impinging on exposed surfaces. Figure 7 illustrates the time history of the air temperature at some peak overpressure levels. The 40-psi point is outside the fireball's maximum radius, so that as the shock strikes, the air temperature is raised about 150°C but cools again within a couple of seconds to nearly normal. At the 100-psi station, which is on the edge of the fireball, the temperature continues to rise somewhat after shock arrival. The shock, being stronger here, heats the air to a higher temperature initially (about 400°C). The air behind the shock is still expanding, but since that air was shocked to even higher temperatures, it exposes the 100-psi point to higher and higher temperatures until the expansion stops. The air flow reverses and eventually ends in the general rising away of the hot remains of the fireball.

The 200-psi point is well inside the maximum fireball radius, and the temperature rise after shock arrival indicates that much hotter air engulfs this station. Here the temperature rises from a shock value of 1000°K ( $\sim 700^\circ\text{C}$ ) to about 4000°K in less than a second.

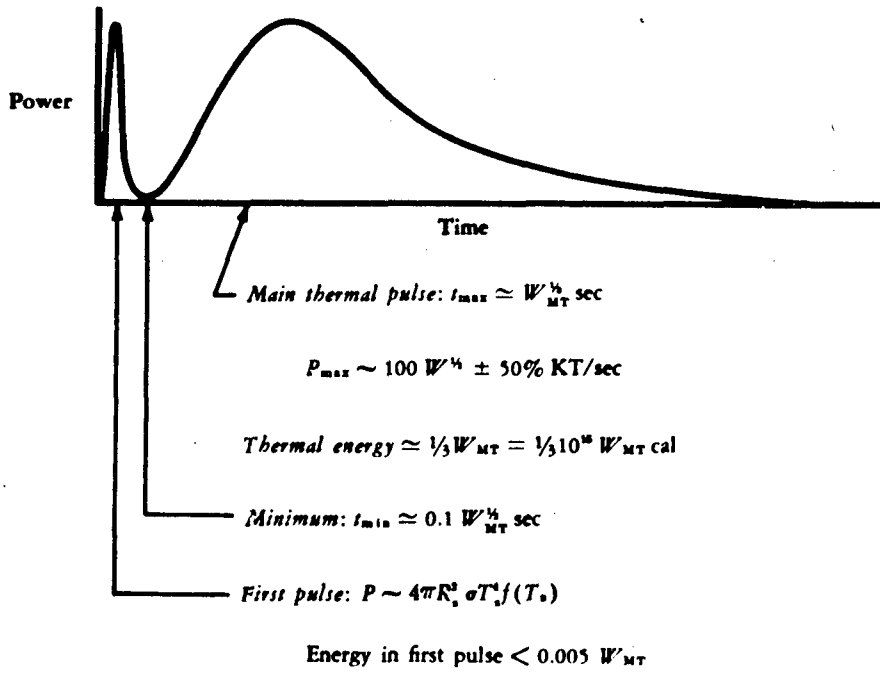


FIG. 6—Thermal Radiation Rate

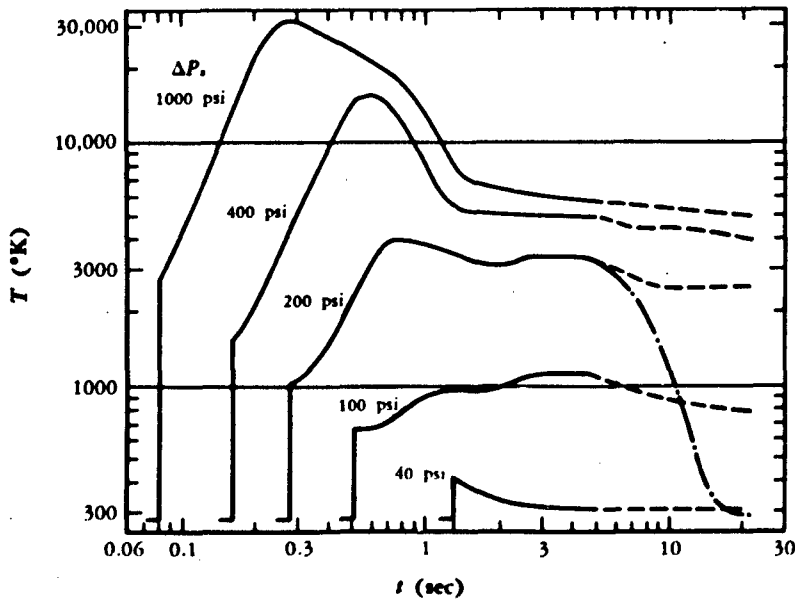


FIG. 7—Temperature versus Time at High Peak Overpressures (1-MT Surface Burst)

Since the fireball is like a bubble in the atmosphere, it begins to rise and pulls away from the earth's surface in only a few seconds. Using a very approximate model for the effect of this fireball rise on the temperature history at the distance corresponding to a peak overpressure of 200 psi, it appears that the hot temperatures of the fireball interior will be reduced at this ground range in approximately the manner indicated by the decreasing tail on the 200-psi curve of Fig. 7. Thus a decrease begins after 4 or 5 sec of exposure, and in 15 to 20 sec the air temperature has returned to normal. The other high-temperature curves would be similarly reduced at late times by the same effect.

At the 400-psi and 1000-psi levels, the temperatures rise even higher but subsequently show a more rapid drop (at times less than 1 sec) because of thermal radiation loss, which becomes significant even before the fireball has begun to rise.

The thermal energy radiated in such relatively short times will result in impressive heat loads on any exposed surface, even far beyond the fireball. From one-fourth to one-half of the yield "shines" away in a matter of seconds. The intensity (measured in calories per square centimeter, or cal/cm<sup>2</sup>) must decrease faster than the inverse square of the distance from the burst because of absorption and scattering in the intervening air.

For purposes of estimating the thermal load from various-yield explosions as a function of distance from the burst, the following approximate formula should suffice for air-burst weapons:

$$Q(\text{cal/cm}^2) = \frac{E_{\text{cal}} T}{4\pi R_{\text{cm}}^2} \approx \frac{10^{12} W_{\text{KT}} T(R)}{12\pi R_{\text{cm}}^2} \approx \frac{W_{\text{KT}} T(D/V)}{D_{\text{mi}}^2},$$

where  $E_{\text{cal}}$  represents the thermal energy emitted (in calories) and is here approximated as one-third of the total yield ( $W$ ) in kilotons (KT);  $D$  is the distance from point of burst in miles (mi);  $R$  is the same distance in centimeters; and  $T$  is the transmission factor. The transmission factor  $T$  in the above approximation depends on the atmospheric conditions and may be estimated in terms of the usual visibility criterion. Recent estimates<sup>(2)</sup> of transmissivities for great distances in clear sea-level air follow approximately the nearly exponential form  $T = (1 + 1.4D/V) \exp(-2D/V)$ . This form is represented in Fig. 8.

The thermal radiation from a surface burst is expected to be less than half of that from an air burst, both because the radiating fireball surface is truncated and because the hot interior is partially quenched by the megatons of injected crater material.

As an example, let us calculate the number of calories per square centimeter to be expected at the distance from a 1-MT surface burst where the blast pressure is 50 psi (about 4400 ft from the burst point or  $\sim 0.83$  mi), for which the transmittance with a 10-mi visibility is about 0.9 (Fig. 8). Entering these numbers in the transmission formula above,

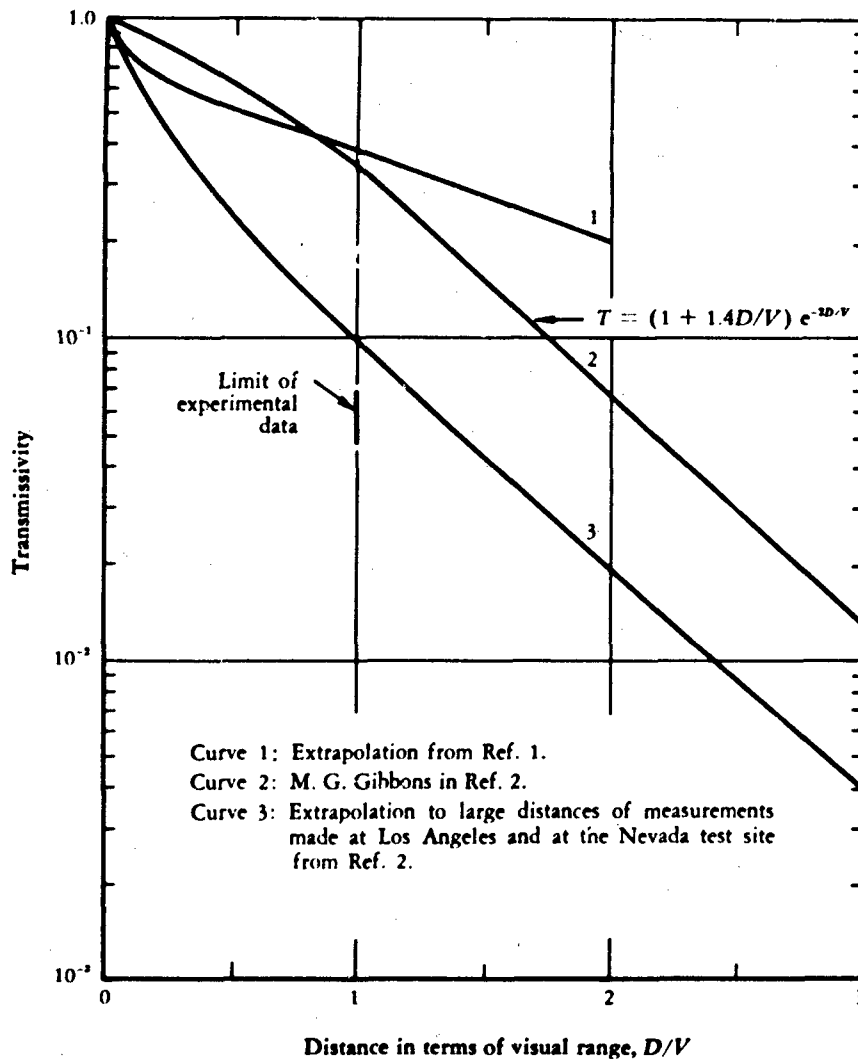


FIG. 8—Transmissivity as a Function of Distance in Units of Visibility

with a reduction of a factor of about one-half for the surface burst relative to an air burst, we obtain something less than 680 cal/cm<sup>2</sup>.

Such degrading factors as attenuating clouds, smoke, haze, fog, dust, or chance shielding by intervening topography, structures, or natural growth further limit the coverage and the exposure at great distances from surface or low-altitude bursts. At a number of miles from low-altitude or surface bursts, even ones of large yield, these combined effects of atmospheric attenuation and obscuration by surrounding terrain features very greatly degrade the thermal loads to exposed surfaces.

Even closer, at the higher levels, heavy thermal damage to protective structures is not expected, since the duration of the heating is too short for appreciable heat conduction beyond

the surface layers of exposed materials. Some pitting and charring, even some evaporation or blowoff from steel or concrete surfaces can occur; but reinforced concrete doors mounted flush with the ground surface do not suffer. Elements exposed above ground level may experience more thermal damage, but most such structures will also be more subject to blast damage.

Inside the fireball the hot air enveloping a protected structure produces a very corrosive environment, but even here, the transient nature of the thermal load works to limit the damage. At typical fireball temperatures, the air itself does not readily transport the radiant energy, and the first vaporized material from the surfaces forms a protective screen that inhibits the subsequent flow of heat to the remaining solid surface. Calculations of thermal damage are necessarily complicated by such obscuration considerations, but observed effects are indeed negligible relative to what simple heat-transfer notions would predict.

Designers must work to avoid damage to door seals or to interiors through contact with the hot fireball gases. Ingestion by ventilating systems and other openings generally must be prevented, but the major design problems do not hinge on the temperature or thermal radiation effects that characterize the fireball. There are other, even more undesirable environmental conditions within the fireball than the brief, but intense, high-temperature exposure.

## IV. NUCLEAR RADIATION

TO ASSESS THE IMPORTANCE of prompt nuclear radiation and to determine the necessary steps for protecting ourselves against it, it is necessary to know (1) the expected level of radiation exposure from a nuclear burst, (2) the efficiency of various shielding materials, and (3) the effects that such radiation can have on both humans and equipment.

Although the initial nuclear reactions (responsible for the energy generation in a nuclear explosion) take place largely inside the bomb and are over in a fraction of a microsecond ( $\mu\text{sec}$ ), some nuclear radiations persist for long periods after the burst and are scattered or radiated from atoms far outside, as well as inside, the bomb debris. Approximately 90 per cent of the neutrons generated are absorbed within the bomb, but the remaining fraction that escapes creates impressive doses in the air. An even larger percentage of the gamma rays emitted during the fission process are absorbed in the bomb, but gamma rays coming from the excited fission-fragment nuclei continue to radiate for a long time. Gamma rays further result from neutron capture in nitrogen—a capture leading to the emission of gamma rays in about 6 cases out of 100.

A bomb may be viewed as the source of a neutron flux roughly proportional to the energy release or yield. The neutron flux (neutrons per unit area, e.g.,  $n/\text{cm}^2$ ) must decrease at least as rapidly as the inverse square of the distance from the explosion source, since the total number of neutrons passing through a spherical surface at any distance does not increase and since the area of the surface increases as the square of the radius. In addition, the flux will be reduced by the removal of neutrons absorbed in the air along the way; and since the number *absorbed* in any distance is nearly proportional to the number *reaching* any distance, an exponential decay in the flux with increasing distance from the point of burst is expected:

$$N(n/\text{cm}^2) \simeq \frac{2 \times 10^{22} W_{\text{MT}}}{R_{\text{ft}}^2} \exp [-(R\rho/780)],$$

where  $\rho$  is the density of air in grams per liter ( $\sim 1.1$  for average sea-level conditions).

When converted to units of rads,\* this formula becomes

$$N = \frac{5 \times 10^{13} W_{\text{MT}}}{R_{it}^2} \exp [-(R\rho/780)] \text{ rads.}$$

The source of gamma rays, being in part dependent on neutron captures as well as on fission-fragment decays, is a more complicated function of both time and space. The fission-fragment radiation decreases with time in proportion to approximately the inverse 1.2 power of time, while the capture gammas are nearly all generated in the first  $\frac{1}{100}$  sec. Although gamma rays traverse the air with roughly the same kind of geometric divergence and absorption behavior as neutrons, the relatively long time for their emission allows the shock movement of the absorbing air to influence the dosage at distant points. This hydrodynamic effect can cause large increases in the gamma-ray dose over the dose that could be expected in the absence of the expanding shock wave. But the effect cannot be important at the most close-in distances, where very little absorbing air lies between source and receiver before the blast. Neither can the effect amount to much at very great distances, where the air motions are both negligible and late. But at the intermediate ranges, where many mean-free-paths of air fill the intervening space (for 1-MT and greater explosions), and where shock motions are impressive, the hydrodynamic effect must be included in any analysis that aims to predict the levels of radiation even approximately.

Since the shock wave is nearly symmetrical about the bomb, it does not influence the spherical character of the gamma-ray flux, but it does change the character of the absorption and scattering (Fig. 9). In a formulation similar to that describing the neutron flux, the hydrodynamic effect can be roughly included by allowing the mean-free-path ( $\lambda$ ) and the effective amplitude of the source ( $\alpha$ ) to be functions of the yield:

$$D_{\gamma} = \frac{3 \times 10^{13} W_{\text{MT}}}{R_{it}^2} \alpha \exp [-(\rho R/\lambda)] \text{ roentgens,}$$

where

$$\begin{aligned} \alpha &\simeq 1 + 0.005 W_{\text{MT}}^2, \\ \lambda &= 1300 + 30W + 3W^2 \text{ ft,} \\ 0.1 &< W_{\text{MT}} < 20, \end{aligned}$$

and  $\rho$  is again the density in grams per liter ( $\sim 1.1$  at sea level).

\*For typical neutron spectra from nuclear explosions,  $n/\text{cm}^2$  is approximately related to units of radiation absorption by the following conversion:  $4.4 \times 10^8 n/\text{cm}^2 \sim 1$  rad, where the rad is defined as the amount of radiation (neutrons) which will produce 100 ergs of absorbed energy per gram of soft tissue. Of the various measures of nuclear radiation intensity, the roentgen unit for gamma rays and the rad for neutrons will be used here. The roentgen represents gamma rays of such intensity that 87 ergs are absorbed in 1 gram of air; but in soft tissue (meat) the same intensity deposits about 97 ergs per gram, or nearly 1 rad.

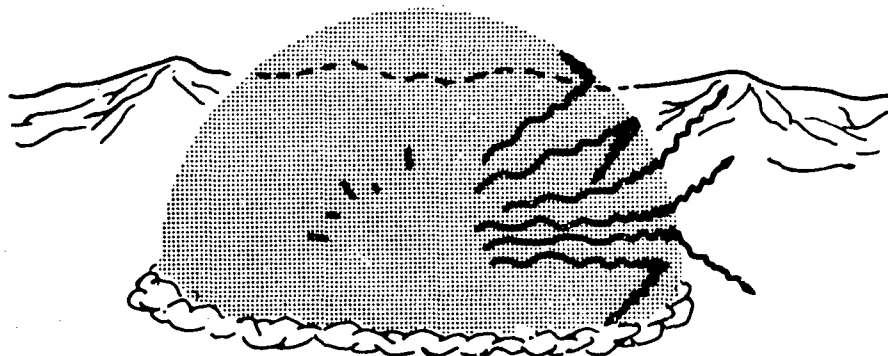


FIG. 9—Shock Influence on Prompt Gamma Rays (a Moving Shield)

Properly, the dose is a more complex function of both yield and range, but over a limited span of yields and for radii corresponding to a few thousand feet, the formula above may suffice.

As an example of the relative gamma-ray and neutron doses, the approximate doses at ½-mi intervals from a 1-MT burst are listed in the table below, together with the approximate overpressure to be expected at those distances. Note that the neutron dose is dominant only at the closest station. Such a crossover between neutron dominance and gamma-ray dominance is to be expected, since the source strength, as well as the amount of absorption with distance, is greater for neutrons.

DOSE VERSUS DISTANCE—1 MT

Distance (mi)	Gamma-ray Dose (roentgens)	Neutron Dose (rads)	Overpressure (psi)
2	~40	~0.5	~10
1.5	~500	~20	~20
1	~10,000	~1,800	~40
0.5	~200,000	~330,000	~200

These numbers reflect the high levels of nuclear radiation present in the air; and to reduce the dose to tolerable levels inside protective structures, some shielding must be done. The functions that shields must perform are obviously related to the nature and intensity of the radiation as well as to the sensitivity and location of the equipment or personnel to be sheltered. Consequently, only some rather general properties of shields or requirements for shielding can be set down without reference to specific targets or attacks.

Since a shield will ordinarily be required to stop both neutrons and gamma rays, it should be designed to include materials appropriate to the absorption of each. Gamma rays are more readily stopped by the heavier elements—the most common being lead, but steel and concrete are also quite efficient. It has been found that for a specified gamma-ray energy, the attenuation depends on the mass of the shielding material. If the linear absorption coefficient is denoted by  $\mu$ , then  $\mu$  divided by the material density  $\rho$  (called the "mass absorption coefficient") is approximately constant. This is strictly true for a monoenergetic gamma radiation for which the attenuation factor may be written as

$$\frac{I_0}{I} = \exp [ (\mu/\rho) \rho x ],$$

where  $I_0/I$  is the attenuation factor of the shield of thickness  $x$ .

For broad radiation beams of polyenergetic gamma rays impinging on thick shields, the gamma photons may be scattered several times, and the emerging radiation intensity may be larger than that given by this equation. In general, however, an effective mass absorption coefficient of 0.021 may be used as a reasonable approximation for materials of low or moderate atomic weight. Thus,

$$\frac{I_0}{I} = \exp (0.021 \rho x),$$

where  $\rho$  is in grams per cubic centimeter and  $x$  is in centimeters.

This latter approximation allows for the buildup due to multiple scattering in thick shields, and is applicable to gamma radiation from nuclear explosions traversing shields of ordinary construction material such as iron, concrete, earth, and stone.

A rough idea of the effect of various common shielding materials on fission-fragment gamma rays can be gained from the thicknesses required to reduce the flux by a factor of 1000. To provide such attenuation takes about 6 ft of earth, 4 ft of concrete, 1 ft of steel, or 6 in. of lead. However, such thicknesses of steel and lead are generally quite costly, and they are commonly used in conjunction with concrete or earth cover. Figure 10 illustrates the slab thicknesses of these various materials necessary to cut the transmitted dose in half for both prompt and fallout gamma radiation.

Shielding for neutron fluxes is not entirely a matter of interposing dense materials but is best accomplished by also including light or hydrogenous elements. Neutrons, as uncharged particles, can move about through heavy atoms like a golf ball bouncing off a row of bowling balls, while, to continue the analogy, a golf ball hitting a pile of other golf balls loses its energy much more rapidly. On each collision of a golf ball (neutron) with a bowling ball

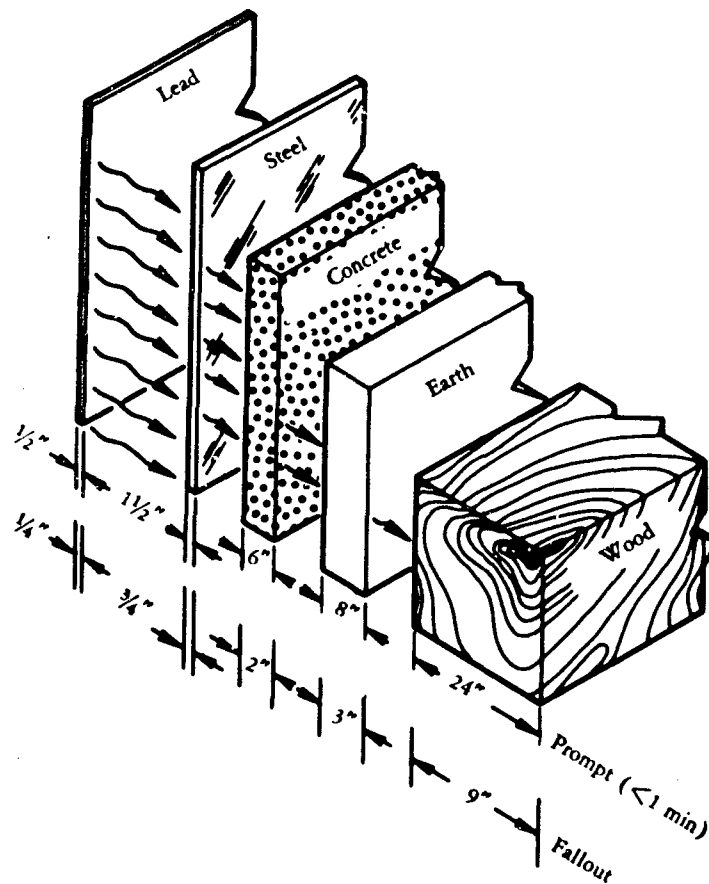


FIG. 10—Half-thickness for Gamma-ray Attenuation

(heavy nucleus), the relative momentum of the two is unchanged, i.e., is conserved. On collision, the massive bowling ball acquires very little of the golf ball's velocity and hence takes very little kinetic energy from the golf ball to conserve momentum. On the other hand, a collision between golf balls usually results in an equal sharing of the initial ball's kinetic energy. Thus on each collision the incident ball (neutron) may lose about half its energy to the stationary ball (hydrogen nucleus).

In this way, a neutron may pass through heavy-element material with little loss in energy, while a neutron in hydrogenous material or matter composed largely of light atomic elements, such as water or plastic or other hydrocarbons, may be slowed down to essentially thermal energies and then may be more likely captured in some nucleus. Shields for energetic neutrons, then, are best designed with light-element components. But in some neutron captures, very energetic gamma rays are emitted; for proper shielding from these, heavier-element material also should be included. A reasonable compromise is often possible with reinforced concrete or special concrete mixtures with iron punchings or boron salts added. For more exotic designs,

laminates of lead and plastics, paraffin, or water are used. Some materials produce radioactive isotopes upon absorbing neutrons, and care should be exercised to avoid elements that have radioactive half-lives long enough to cause continued danger. It is well to note that the first few inches of shield may reduce the neutron flux more than succeeding inches, since the first inches screen out many low-energy or "slow" neutrons (whose cross section for capture is generally higher than that for high-energy or "fast" neutrons), leaving only fast neutrons to traverse succeeding inches of the shield.

The attenuation factor of a beam of neutrons by a shielding material may be written as

$$\frac{N_0}{N} = \exp(\Sigma x),$$

where  $N_0/N$  is the ratio of the radiation dose which would have been received in the absence of the shield to the dose received behind the shielding material;  $\Sigma$  is related to a macroscopic cross section (equivalent to the linear absorption coefficient of gamma rays) and is experimentally determined to be  $0.1 \text{ cm}^{-1}$  for water,  $0.09 \text{ cm}^{-1}$  for concrete, and  $0.16 \text{ cm}^{-1}$  for iron concrete; and  $x$  is the shield thickness in centimeters. Thus, except in the first few inches where the effectiveness of the shield is even greater, it takes about 10 in. of concrete to reduce the flux by a factor of 10, or about 20 in. to cut it by a factor of 100. Special heavy concrete may be as effective in thinner layers, 7 in. being roughly equivalent to 10 in. of normal concrete. The use of colemanite or other boron salts in the mix can result in even greater absorption capability, since one of the natural isotopes of boron has an unusual affinity for the slow neutrons.

For many, but not all, situations, the necessary earth cover or concrete and steel for blast protection is more than a sufficient radiation shield. To determine the amount of shielding required at an installation, the possible effects of such radiation on humans and on equipment should be known and tolerance levels determined. Although the response of biological systems is not directly proportional to the energy absorbed, the neutron dose in terms of rads will serve as a rough measure of allowable human doses. Doses of more than 450 roentgens or rads may be expected to kill 50 per cent of those exposed, and a dose of over 700 roentgens will cause 100 per cent fatalities; but a dose of less than 100 roentgens is not expected to cause noticeable degradation of human activity and is not likely to be lethal. Consequently, in the design of areas where personnel will be protected during attack, the accepted dose should be kept below 100 rads or roentgens. Something less—say, on the order of 50 rads—would be preferable for design purposes, since the prompt radiation dose is likely to be supplemented later by fallout doses.

Electronic systems must also be protected from intense radiation. Circuits involving semiconductors are particularly sensitive, but the level of allowable radiation is fairly sensitive to details of the circuitry. A broad rule for currently typical electronic systems is that for silicon elements the neutron exposure should be kept to less than  $10^{11}$  n/cm<sup>2</sup>, and for germanium elements, to less than  $10^{12}$  n/cm<sup>2</sup>. Usually diode applications are less sensitive than higher modes of operation, and thin transistors are less sensitive than thick ones. With special attention to circuit design, both thresholds for permanent damage can be increased by at least a power of 10.

The only structural materials exhibiting particular sensitivity to radiation are synthetics such as Teflon, which may be damaged by exposure to more than  $10^5$  roentgens (gamma rays).

## V. ELECTROMAGNETIC PULSE

**STRONG ELECTROMAGNETIC SIGNALS** are observed from nuclear explosions. These signals, which extend through the entire radio and radar spectra, are a result of the intense ionizing radiation from the nuclear reactions and their asymmetries and earth-field interactions.

Where electronic equipment in a protected system is required to operate continuously throughout a nuclear attack, care must be exerted to provide magnetic shielding and electrical isolation from transients induced in external conductors.

If an installation involves long lines of conducting cables, or extensive wired connections beyond a localized facility, some provision should be made for protection against permanent damage due to excessive currents induced by the low-frequency component of the electromagnetic pulse. Such pulses and protective provisions may be thought of as quite analogous to those for natural lightning strokes.

The induced pulses are in general characterized by high power but low energy, which is the consequence of their highly transient nature. However, very-low-frequency components of the pulse may exist to such an extent that both electric and magnetic fields may be propagated to considerable depths below the earth's surface (corresponding to large "skin depths"). Electronic gear that responds adversely to such very-low-frequency field changes should be mounted and protected with these phenomena in mind.

## VI. CRATERING AND DIRECT GROUND SHOCK

### CRATERING

THE CRATER that results from a nuclear detonation on hard rock has dimensions roughly 20 per cent smaller than those of a similar burst on soil or soft rock; i.e., a burst on rock excavates a crater volume only about one-half of that expected from a burst on soil. The efficiency of cratering by nuclear explosives depends on more than just the nature of the medium (hard rock, soft rock, dry soil, saturated soil, etc.); it varies also with the depth of burst and with the yield of the explosive, and is further sensitive to some details of the weapon and of its immediate surroundings at the instant of detonation.

The effect of depth of burst is particularly dramatic for nuclear explosives near the surface. The relatively small mass and physical dimensions of a nuclear charge (in comparison with the mass and size of its high-explosive equivalent) makes the crater from a low air burst or contact burst much less impressive, while for an adequately buried and tamped nuclear charge, the surrounding earth in large part compensates for the disparity in explosive mass and size. The dependence of crater radius and crater depth on depth of burial of a 1-KT nuclear charge is illustrated in Fig. 11. Some typical data points are included. The sharp change in crater efficiency at the exact surface of the earth is exaggerated.

Crater dimensions may be approximately scaled for other-yield weapons by multiplying depth by the fourth root of the yield ( $W^{0.25}$ ) and diameter by the yield to the three-tenths power ( $W^{0.30}$ ). Such an empirical scaling is used in Fig. 12 to approximate crater dimensions for three types of bursts in hard rock: for surface or contact bursts, for shallow-buried bursts, and for bursts buried deep enough to maximize the crater volume.

Theoretical work in recent years has contributed considerably to an understanding of the cratering action of nuclear explosives. Viewed in axial symmetry, the early soil dynamics has been modeled with two-dimensional hydrodynamic numerical methods. Such a model is far from complete. The use of hydrodynamics is strictly justifiable only in that region where the ground medium is subject to stress well in excess of its shear strength, while final crater

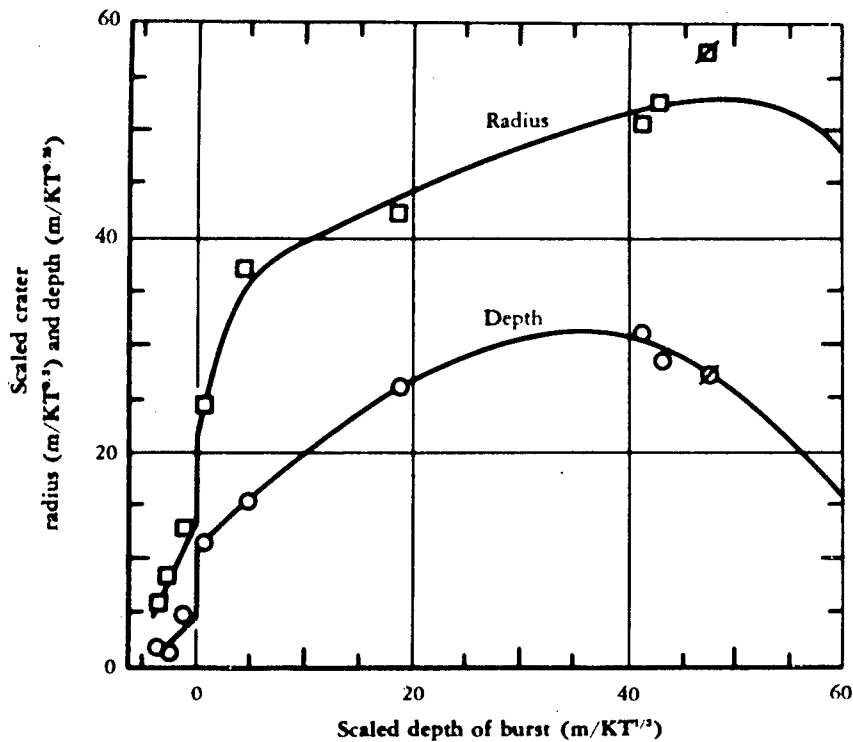


FIG. 11—Crater Dimensions versus Depth of Burst (1 KT)

dimensions are likely to be influenced as much by the subsequent lesser stresses and motions characteristic of solids under compression and shear.

The extremely high energy densities and temperatures of a nuclear explosion guarantee the validity of a hydrodynamic treatment in studying close-in soil response, since the initial strong shock will vaporize the earth for some distance. Because the geometry of the burst relative to the interface separating ground and air strongly influences the formation of a crater, a hydrodynamic model in two dimensions, including vertical and radial motions, is vital to a description of pressures and velocities during and following crater formation.

Although such a calculation may include the effects of both the high pressures of the bomb-vapor residual energies and the pressure or impulse from the air-blast slap (see Fig. 13 on page 24), early results have shown that only the extremely-high-pressure impact of the bomb material itself is important in the excavation process. The air slap does indeed send a shock into the ground, but it is over a wide area and at pressures several orders of magnitude less than those in the direct shock out of the bomb. While the air blast is born in a great fireball, which begins pushing on an area many times that of the eventual crater, the remaining energy in the bomb vapors is so concentrated as to vaporize and eject quite force-

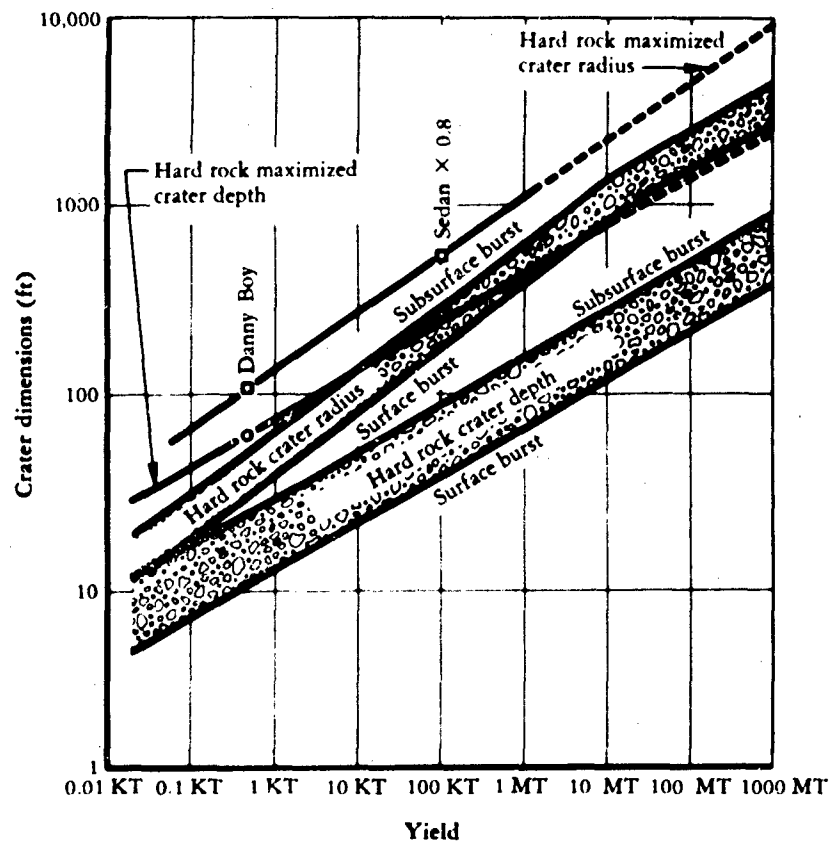


FIG. 12—Crater Scaling

fully the immediately surrounding material. Out along the surface beyond the region of the crater, the air-blast slap will induce ground stress that will exceed any stress directly propagated that far from the initially intense bomb shock (which arrives later); but for the cratering action, and for shocks immediately below the crater, the effect of air slap is truly negligible.

Thus the internal and kinetic energies delivered directly to the ground from the bomb are a most important aspect in forming a near-surface-burst crater and inducing ground motion below it. For this reason, the precise height or depth of burst and the details of the bomb disassembly have an important influence on the crater and on the energy initially delivered into the soil. Shallow burial and denser bomb cases may enhance the cratering efficiency by very significant factors.

A true contact burst might be expected to deliver half its momentum downward into the soil and half upward into the air. However, only a fraction of the bomb energy finds its way into kinetic motion of the bomb materials. Further, since the soil is at least a thousand times

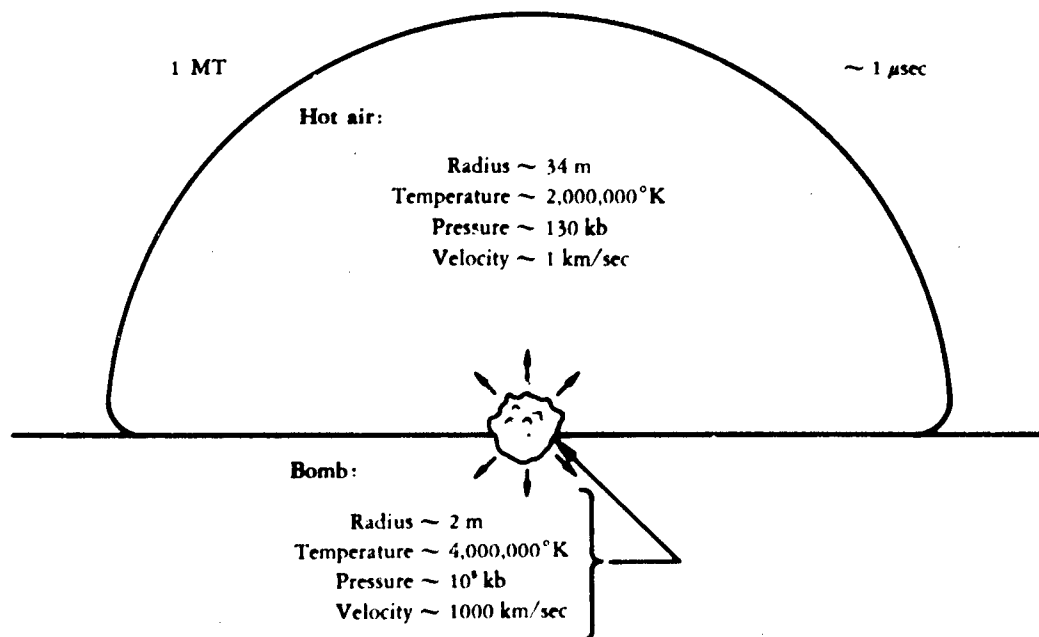


FIG. 13—Initial Conditions for Surface-burst Cratering Motion

denser than the air, the dynamics of a surface burst require for conservation of momentum that the velocities imparted to the soil be less than those created in the air by just this ratio of densities. The kinetic energy imparted in this way will be proportional to the square of the velocity, and so will be proportionately much less in the dense material. In one example, something like 15 per cent of the energy from a 1-MT surface explosion started out into the ground.

Figure 14 illustrates the pressure contours typical of a surface burst of a few megatons on a relatively soft volcanic rock material at about  $\frac{1}{10}$  ms after detonation. Pressures are in kilobars (kb), so that the pressures shown run to several megabars (Mb). The early response is centered in a downward hemispherical shock several meters below the burst point. The presence of the surface has already caused some relief of pressure at shallow depths, but the main shock appears to be fairly uniform and spherically diverging in a vertical cone about 90 degrees (deg) in width.

Figure 15 illustrates a velocity field at this same early time, with the same portion of a spherical shock appearing. Rock vapor is already streaming upward at velocities of several tens of meters per millisecond (or tens of kilometers per second).

At a time of some 50 ms, a relatively late time in the cratering action, the pressure contours still show much the same curved shock with continued surface relief (Fig. 16).

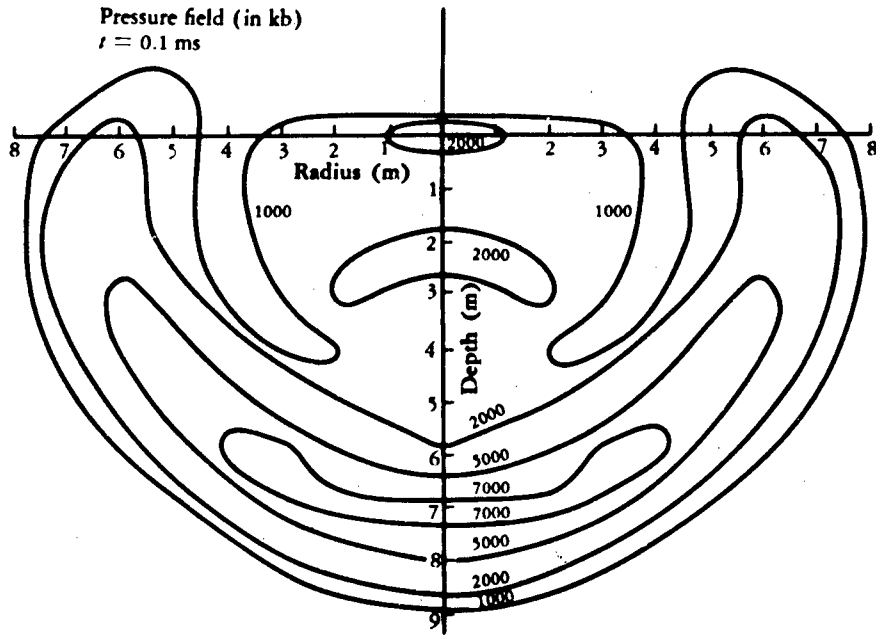


FIG. 14—Earth Pressure Contours from Surface Burst ( $t = 0.1$  ms)

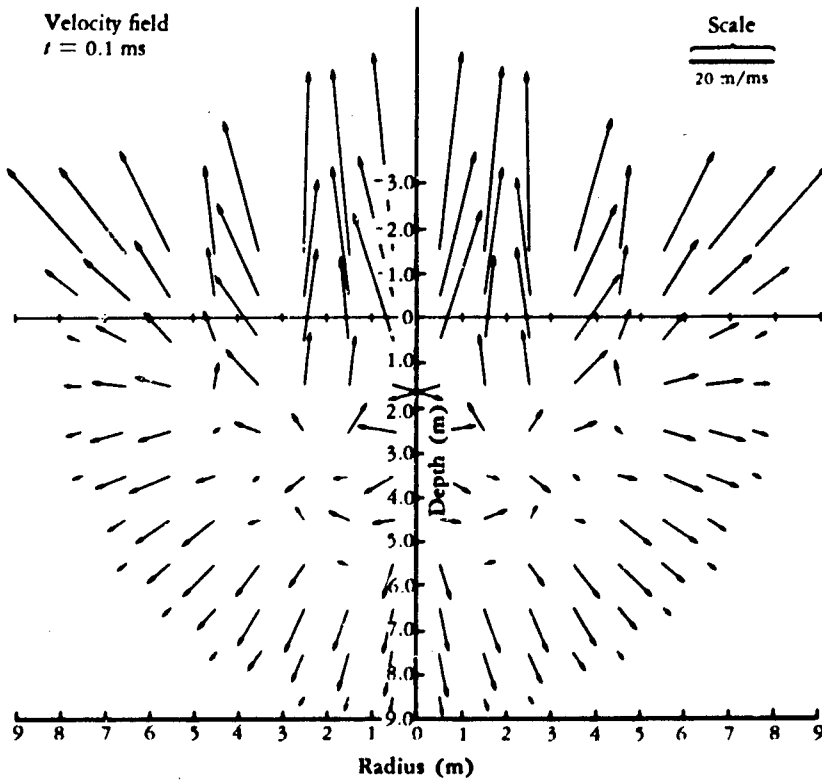


FIG. 15—Particle Velocities from Surface Burst ( $t = 0.1$  ms)

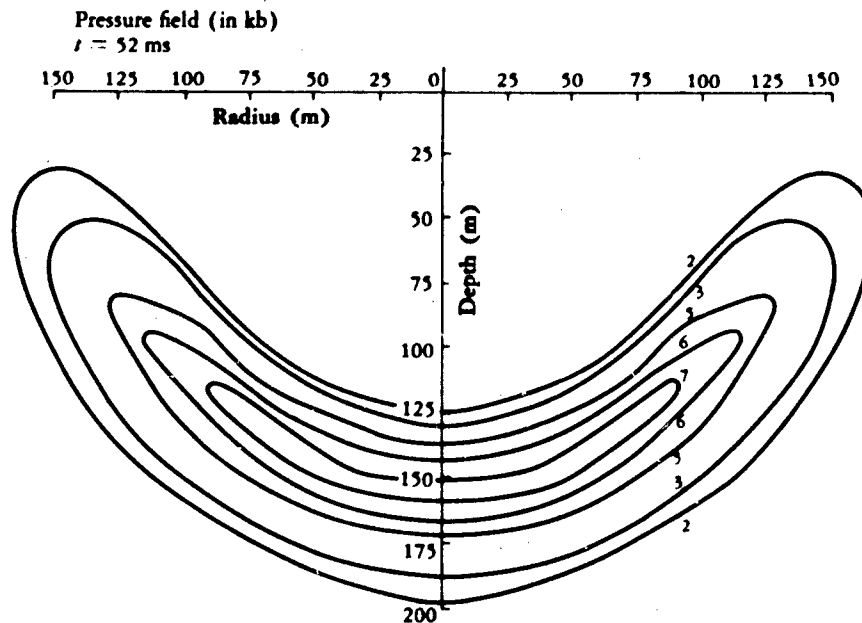


FIG. 16—Earth Pressure Contours from Surface Burst ( $t = 52 \text{ ms}$ )

The shock strength is now down to about 7 kb at a depth of 160 m, and pressures are approaching a level where hydrodynamics should give way to consideration of the solid-state properties of the rock—the medium no longer being a true fluid. But carrying the calculation further may lead to reasonable first-motion information (i.e., peak velocities and stresses), in spite of the failure of the fluid model to include the elastic or plastic properties of a solid. In Fig. 17, the velocity vectors at about 50 ms show the same spherical nature, with the high-speed jetting above the surface typical of such a burst. Figure 18 shows a continuation of this problem to 100 ms, where the shock pressures are perhaps 3 kb at a depth of 250 m ( $\sim 800 \text{ ft}$ ). These are pressures of an awkward level to treat: too high for clearly elastic propagation and too low for hydrodynamics to be rigorously applicable in many earth materials. Crushing, plastic, and viscoelastic behavior could be expected to have important influences on both the subsequent wave propagation and on the response of an imbedded structure. In this analysis, the portion of the shock running vertically below the burst point remains the strongest; and it may represent a significant limitation to the survivability of structures directly underneath a large-yield explosion.

The corresponding velocity field of this 100-ms time is shown in Fig. 19 (page 28). A gratifying, if fortuitous, aspect of the velocities at both this time and the previous 50-ms time is the rather clear division of upward and downward motion by a contour not unlike that which represents the expected final crater profile.

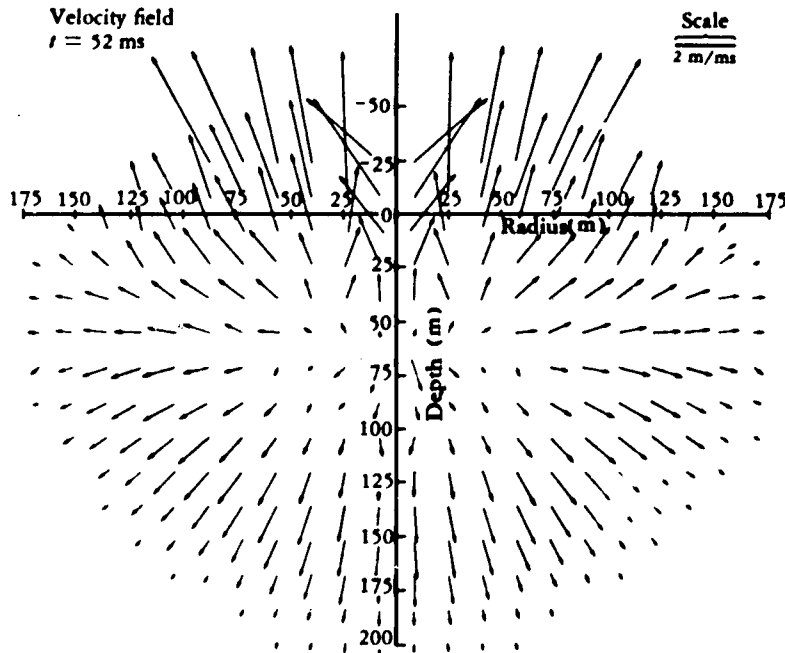


FIG. 17—Particle Velocities from Surface Burst ( $t = 52 \text{ ms}$ )

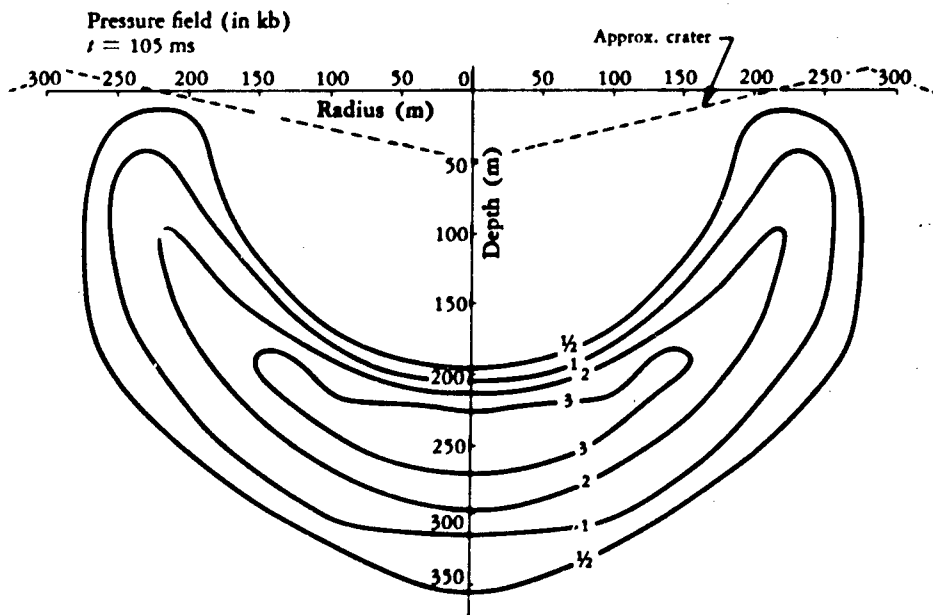


FIG. 18—Earth Pressure Contours from Surface Burst ( $t = 105 \text{ ms}$ )

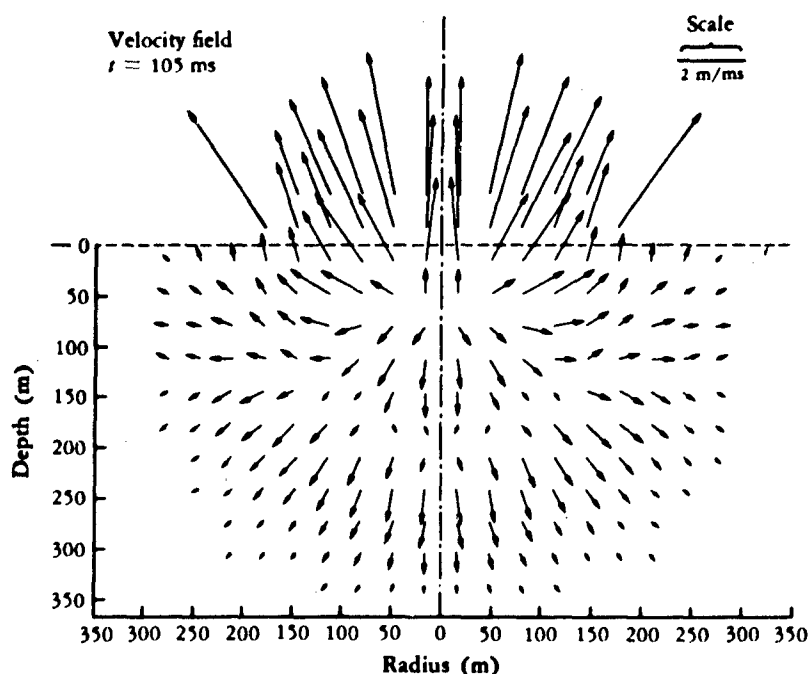


FIG. 19—Particle Velocities from Surface Burst ( $t = 105 \text{ ms}$ )

#### DIRECT GROUND SHOCK

These calculational results are not sufficiently accurate at low stress levels to provide direct predictions of peak earth stress beneath such a crater, but they are useful in manipulating data from buried bursts to provide such estimates.

Figure 20 presents some rather arbitrary bands of peak earth stress as functions of the depth below surface bursts of 1, 10, and 100 MT.

It should be noted that the early decay of peak pressure follows an inverse cube of the slant distance from the burst point, as expected for a strong shock in any medium. At the lower pressures, the decay approaches a more gradual decay—more like the inverse square or inverse three-halves power of the radius. The pressures shown are intentional overestimates based largely on the hydrodynamic calculations. Experience with contained explosions indicates that other dissipative mechanisms provide an even more rapid decay of peak stress with distance.

Based in large part on these early calculations, Fig. 21 shows peak stress contours for both a surface and a shallow-buried burst of 1 MT. The levels from  $\frac{1}{2}$  to 2 kb correspond to the onset of gross rock failures for most formations and thus represent the range of survival for the best examples of underground construction. From the relatively small lateral

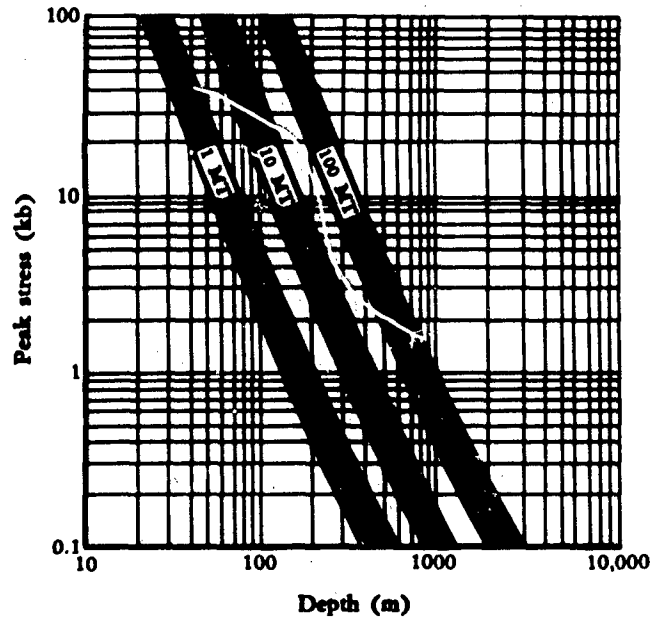


FIG. 20—Peak Stress versus Depth in Hard Rock (beneath Surface or Shallow-buried Bursts)

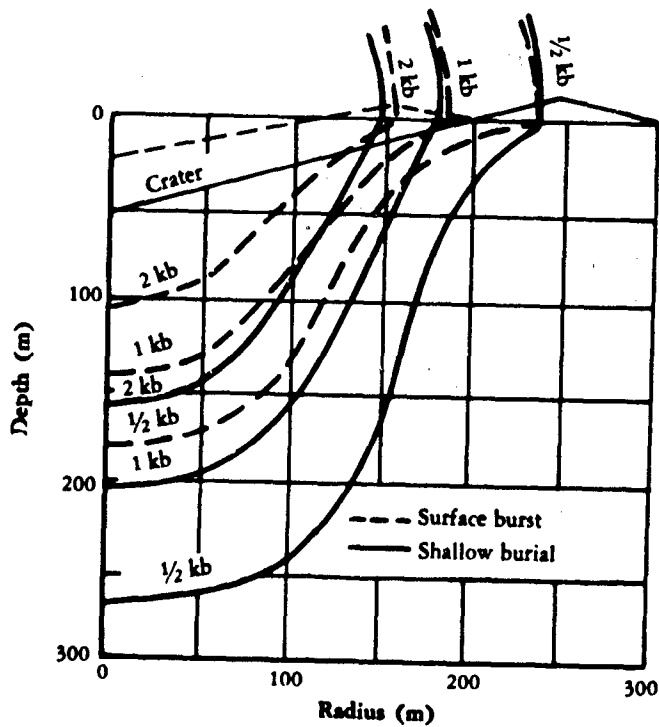


FIG. 21—Peak Stress Contours for 1-MT Hard Rock

extent of these contours it is clear that a weapon must be delivered with great accuracy to be effective against a structure set deep in hard rock. Further, even a direct hit will not destroy an installation that is deep enough. Since these dimensions should increase no faster than as the cube root of the yield, an increase in attacking weapon yield does not rapidly require excessive depths of burial.

## VII. AIR BLAST

### SHOCK PARAMETERS

RETURNING TO THE HISTORY of the blast, we see in Fig. 22 the overpressure profiles extended to later times, larger distances, and lower overpressure levels. The pressure-time relationship may be more easily understood by noticing the nature of these profiles at the earlier times (before 1 sec). Note that at these smaller radii the pressure drops rapidly just behind the shock, while in the interior there are essentially no pressure gradients. The interior is the very hot region of the fireball where pressure pulses of any sort are transmitted outward very rapidly because of the high sound speeds accompanying these high temperatures. Near the front, however, the positive pressure gradient (as a function of radius) is a necessary feature of the spherically expanding shock, in which the interior gas is constantly decelerated as the shock runs into more and more stationary air.

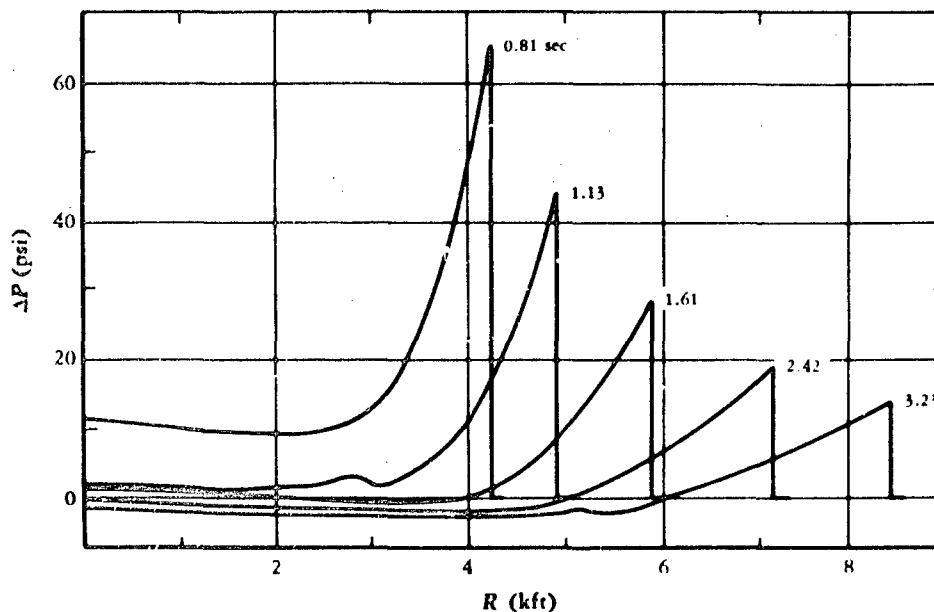


FIG. 22—Overpressure versus Radius (1-MT Surface Burst)

Figure 23 shows the shock arrival time  $t_s$  and the shock radius  $R$  for various overpressures resulting from the detonation of a 1-MT bomb. These values depend on the energy of

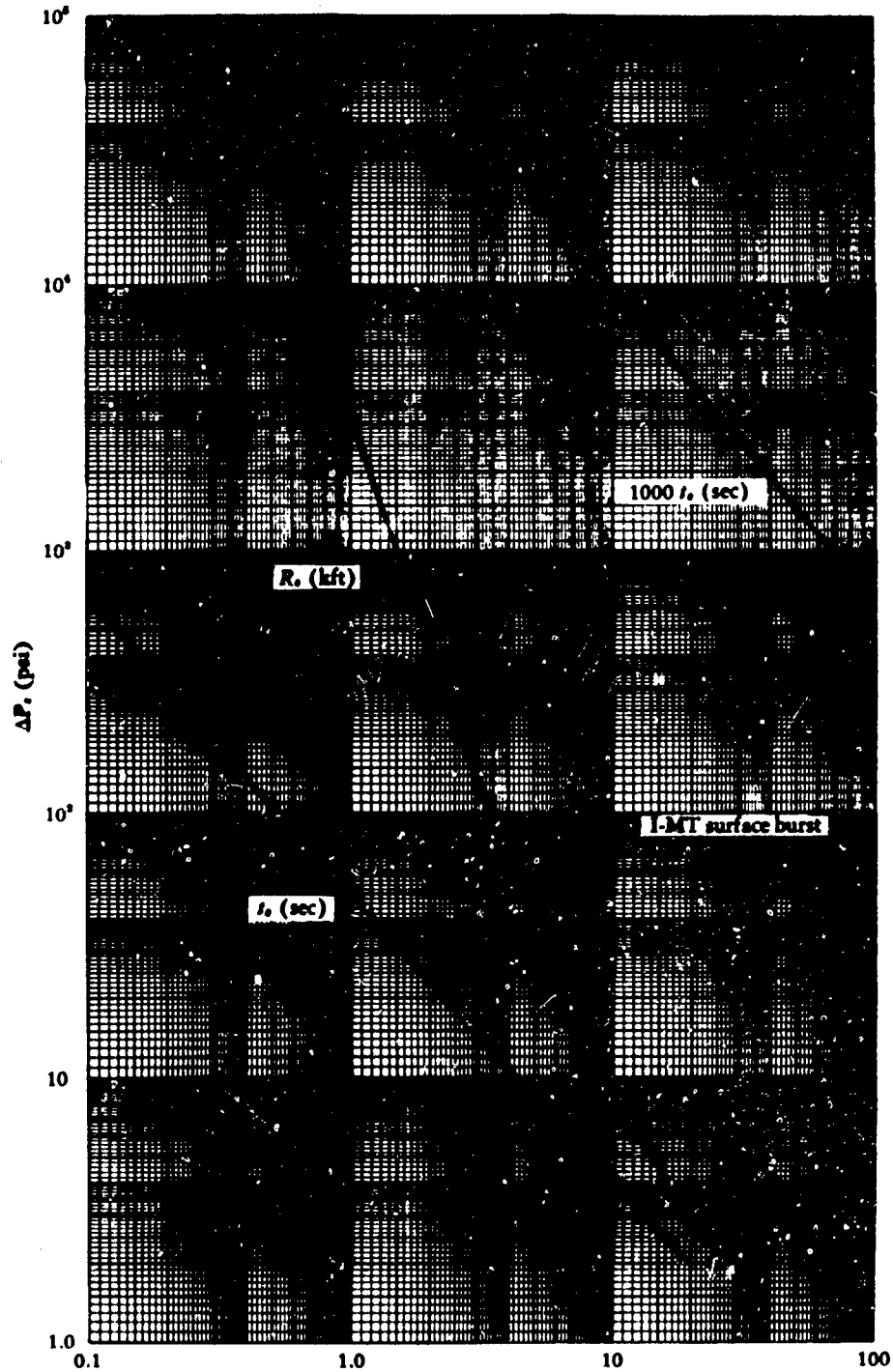


FIG. 23—Shock Radius ( $R_s$ ) and Arrival Time ( $t_s$ ) versus Peak Overpressure for a 1-MT Surface Burst

explosion, being greater by the cube root of the yield in megatons for yields greater than 1 MT. On shock arrival the pressure jumps within a fraction of a millisecond (or within a few milliseconds to tens of milliseconds for precursed shocks) to the peak pressure. The subsequent decay of the pressure pulse is initially dominated by the passage of the pressure spike associated with the shock front itself. As the spike moves on, the continuing decay is dictated by the general rate of pressure decrease in the more uniform shock-wave interior, which has by then engulfed the position in question. This time history can be quite well described at all pressure levels by the sum of three decreasing exponential functions of the time:

$$\Delta P = \Delta P_s (ae^{-\alpha\tau} + be^{-\beta\tau} + ce^{-\gamma\tau})(1 - \tau),$$

where  $\tau$  is the time after shock arrival measured in units of positive phase duration.

To force this curve to go to zero overpressure at the end of the positive phase, a linear factor has been included that becomes zero at a time equal to the duration of the positive phase ( $\tau = 1$  or  $t = D_p^*$ ), where time is measured as the time after shock arrival.

Figure 24 gives the values of all shock parameters and coefficients necessary to obtain the pressure-time curve for a given peak overpressure. For example, at  $\Delta P_s = 1000$  psi and  $W = 1$  MT, these values are

$$\begin{aligned} \tau &= \frac{t - 0.070}{1.20}; \\ a &= 0.15, \quad b = 0.30, \quad c = 0.55; \\ \alpha &= 2.90, \quad \beta = 21, \quad \gamma = 130; \end{aligned}$$

and

$$\Delta P(t) = 1000(0.15e^{-2.90\tau} + 0.30e^{-0.21\tau} + 0.55e^{-130\tau})(1 - \tau).$$

Similarly, Fig. 25 (page 35) gives the shock parameters and coefficients for obtaining the dynamic pressure-time curve based on the analytical fit

$$Q = Q_s(1 - \omega)^2(de^{-\delta\omega} + fe^{-\phi\omega}),$$

where

$$\omega = \frac{t - t_s}{D_u^*},$$

$D_u^*$  = duration of positive velocity ( $\sim W_{MT}^{1/3}$ ),

$Q_s$  = peak dynamic pressure.

At 1000-psi overpressure, for example,  $D_u^* = 2.5$  sec and  $Q_s = 2900$  psi;  $d = 0.32$ ,  $f = 0.68$ ;  $\delta = 150$ ,  $\phi = 350$ ; and  $Q(t) = 2900(1 - \omega)^2(0.32e^{-150\omega} + 0.68e^{-350\omega})$ .

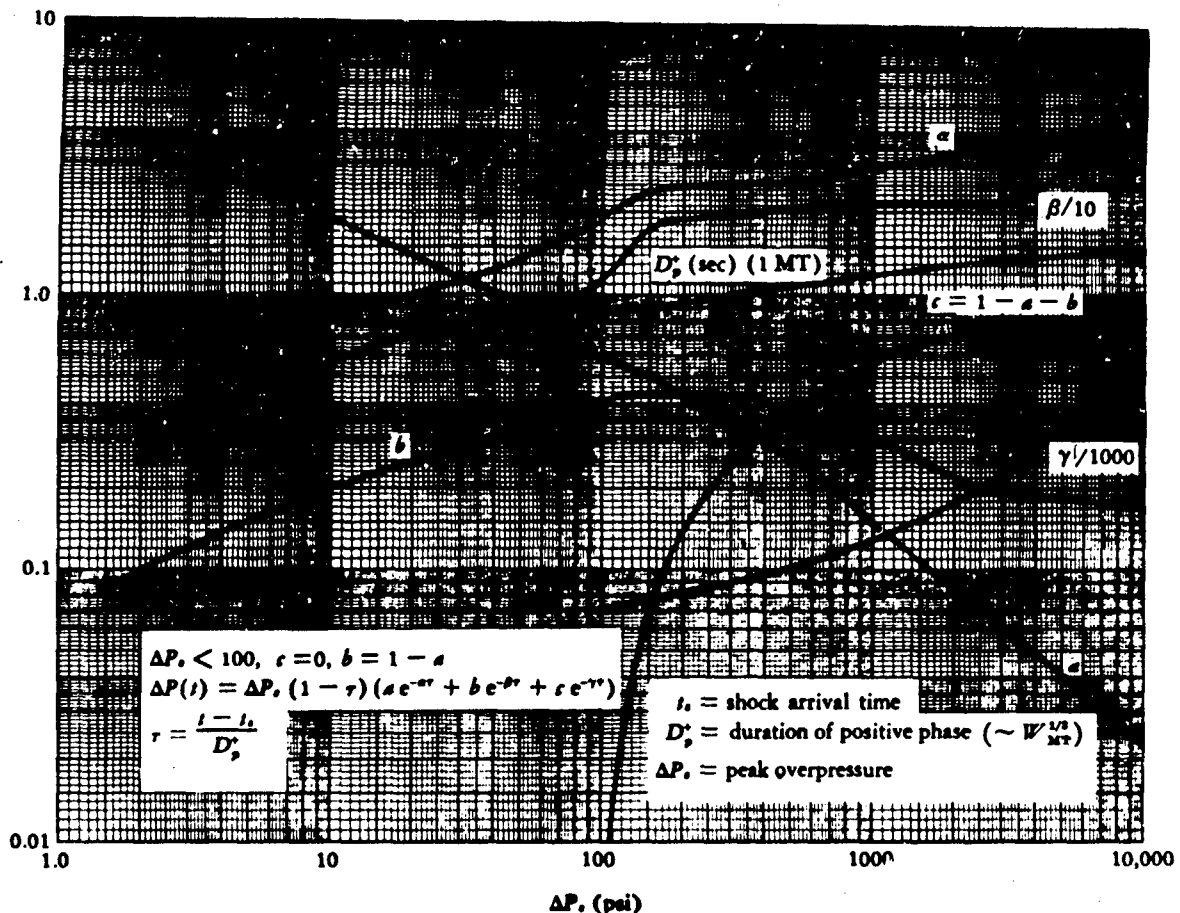


FIG. 24—Approximate Analytic Form for Overpressure versus Time for Nuclear Blast Wave in Terms of Peak Overpressure

Curves showing the pressure-time relations based on these analytic expressions are given in Fig. 26 (page 36) and Fig. 27 (page 37).

Figure 28 (page 38) displays the positions of the shock front from a 1-MT surface burst, illustrating very generally the relative position of the fireball and crater. The higher peak overpressures at distances closer to the burst point are strikingly evident. Note that 100 psi occurs just at the edge of the fireball. The high transient winds or air velocities accompanying the shock emphasize the importance of placing protective structures below, or at least flush with, the surface. The short solid lines below the ground indicate schematically an expected attenuation of peak overpressure with depth at a given range; the dashed lines are intended to indicate the general relations between the air-shock position and the wave front in the soil at corresponding times. At the higher overpressures (down to 200 or 300 psi) the air-shock speed is faster than the seismic velocity of most soils, so that the compression wave in the soil lags behind

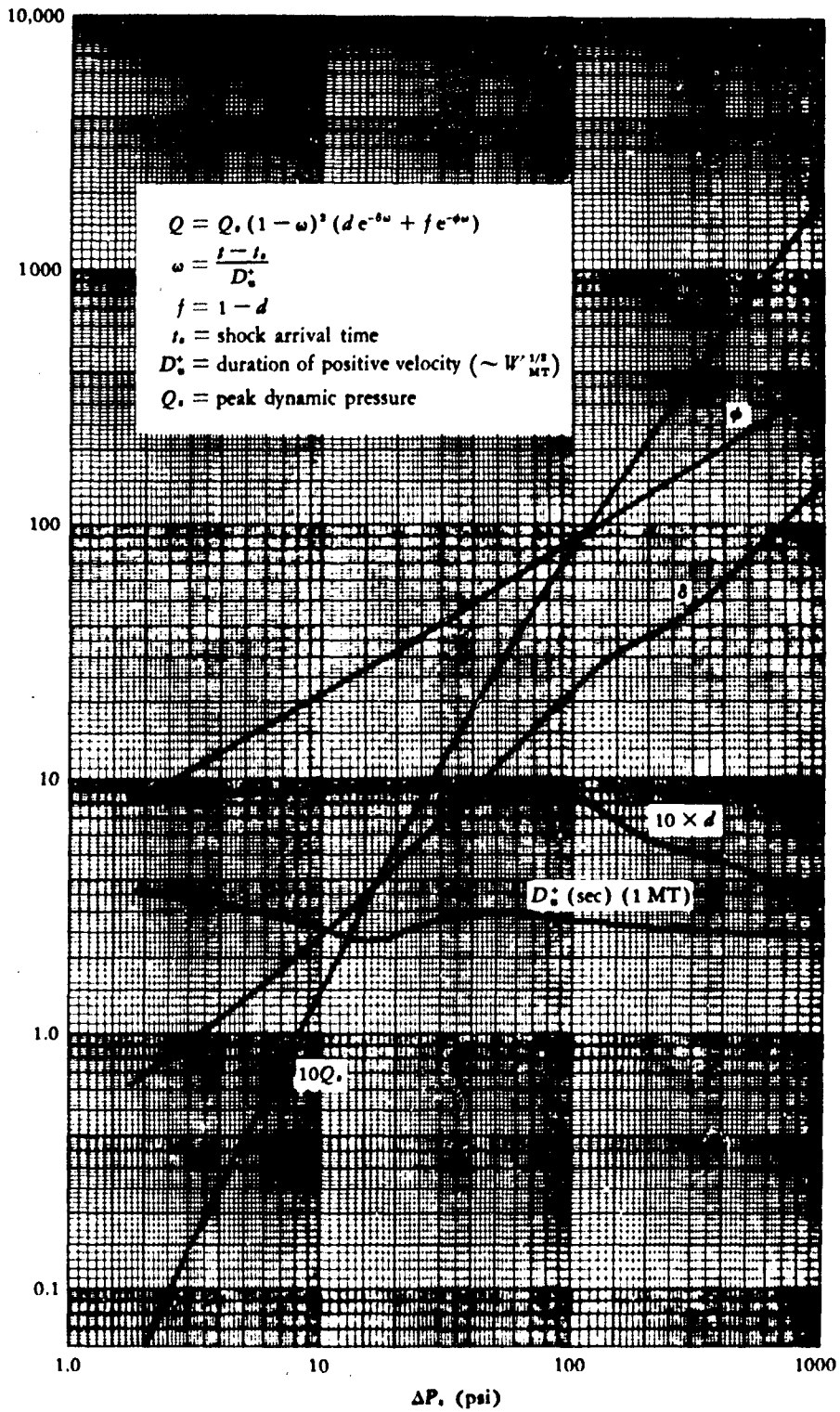


FIG. 25—Approximate Analytic Form for Dynamic Pressure versus Time for Nuclear Blast Wave in Terms of Peak Overpressure

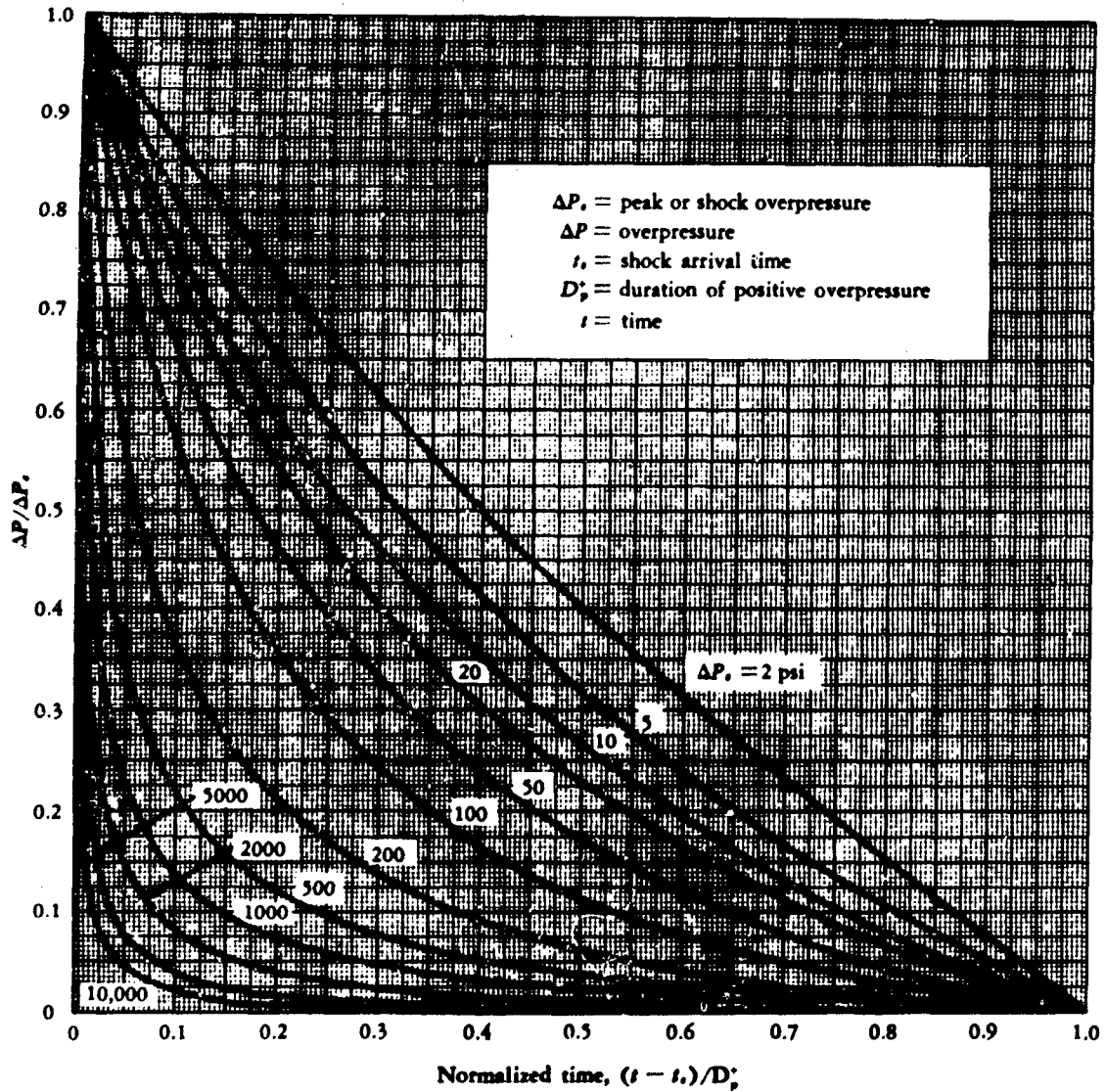


FIG. 26—Form Factors for Overpressures from Nuclear Explosions

and propagates downward from the surface along a shallow saucer-shaped wave front. As the air-shock speed decreases, at some point it must drop below seismic speeds, thus allowing waves in the soil to move out faster and so to move ahead of the air blast. This feature leads to some complication in both the air-shock and the ground-shock interpretation. More about the latter is included below in the discussion of ground shock.

Some general features of an ideal or normal blast wave are illustrated as a function of the peak overpressure in Fig. 29 (page 39). Independent of weapon yield, the shock temperature, peak dynamic pressure, shock velocity, and maximum particle velocity at any point are related to the peak overpressure at that point as shown in this graph. The temperature and

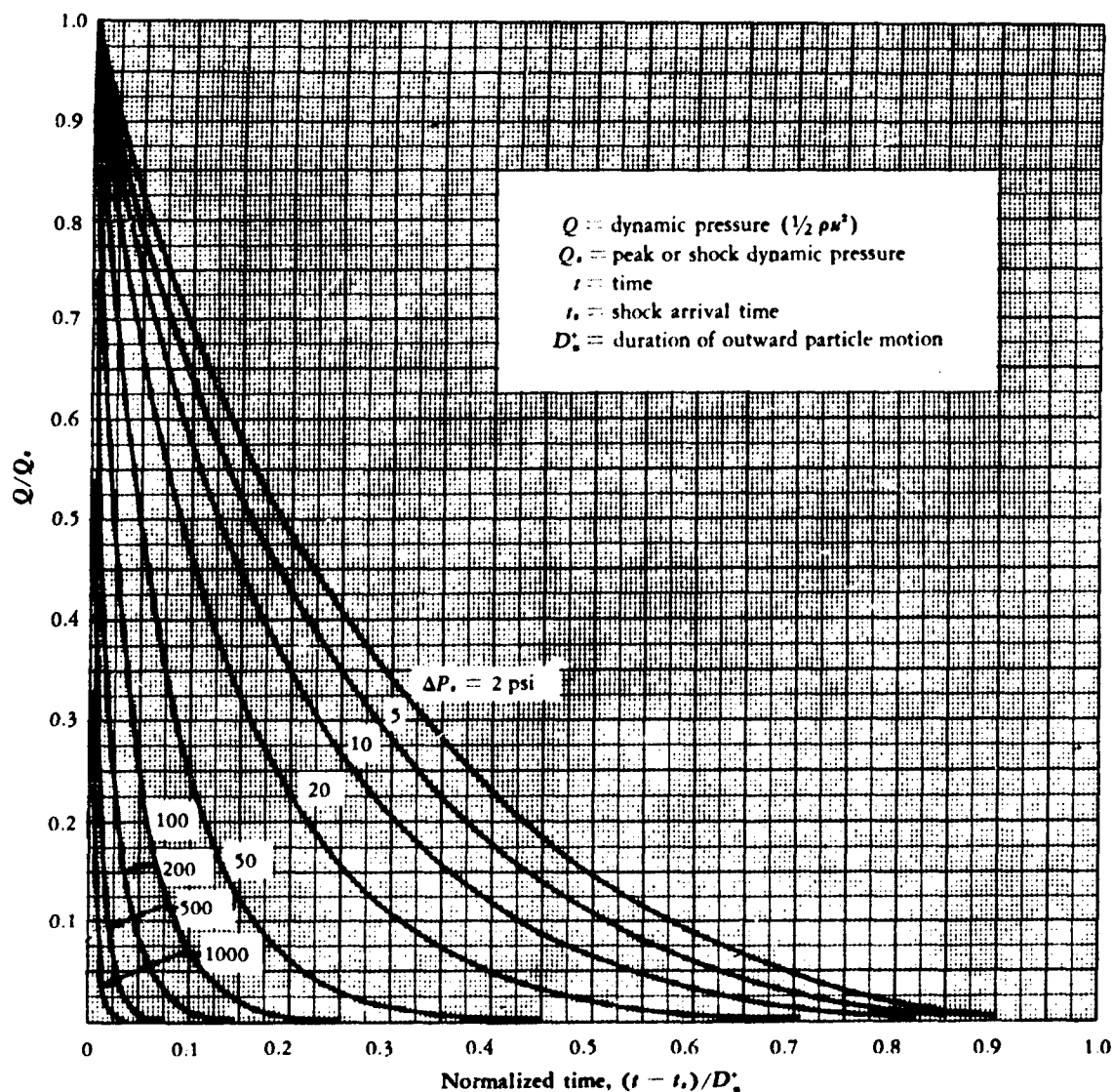


FIG. 27—Form Factors for Dynamic Pressures from Nuclear Explosions

velocities increase with increasing peak overpressure, but they increase less rapidly than the peak overpressure itself. The peak dynamic or wind pressure rises very rapidly, however—more like the square of the peak overpressure at low overpressures—and is proportional to the overpressure itself only at the highest level.

The impulse of the blast wave is often a significant parameter in damage prediction. The impulse here is defined as the time integral of the pressure taken over the duration of the positive phase. Figure 30 (page 40) shows the general relation of the impulses for overpressure and dynamic pressure (along with the durations of each) to the peak overpressure. From this figure

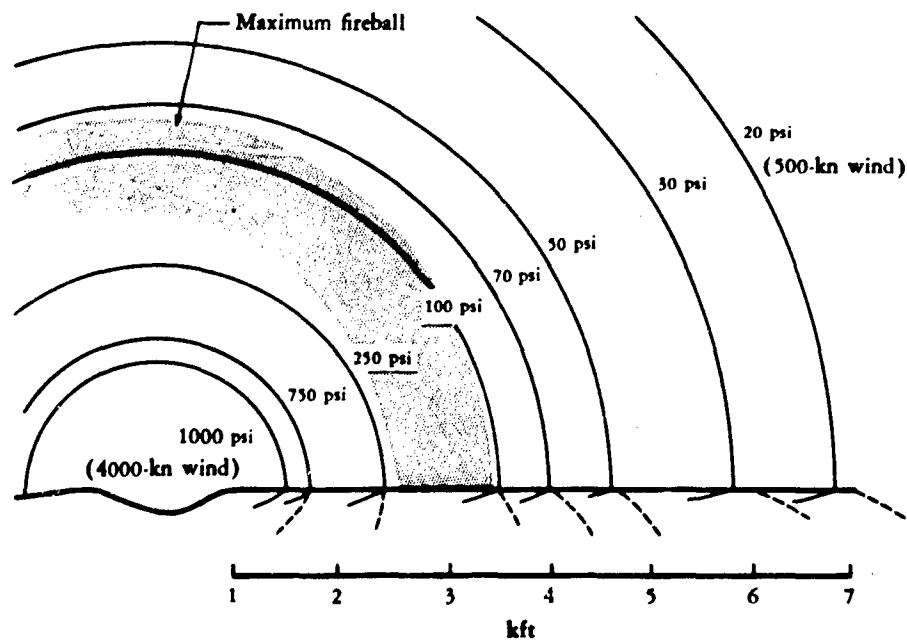


FIG. 28—Shock-wave Peak Pressures (1-MT Surface Burst)

it can be determined that the overpressure impulse increases (with increasing overpressure) approximately as the square root of the overpressure below 1000 psi, and as the cube root at higher overpressures. Since at the higher overpressure levels the overpressure itself is proportional to the inverse cube of the radius, its impulse then is roughly proportional to the inverse radius. The dynamic pressure impulse decreases only very slowly with decreasing overpressure above 100 psi—being proportional in that region to about the fourth root of the overpressure—but it drops in importance very rapidly at lower overpressures.

Although the total durations of the positive phase of overpressure and air velocity do not change greatly with overpressure, at the higher overpressures the bulk of the impulse is delivered largely in the first few milliseconds rather than uniformly over the whole positive phase. As illustrated previously in the pressure-time curves, the pulse shapes at high overpressures are much more peaked than at lower overpressures, and the exact duration of the positive phase is less important there than it is at the lowest overpressure levels (where the pulse becomes nearly linear in its time decay).

#### BLAST LOADING ON STRUCTURES

A knowledge of the characteristics of an air blast propagating along the ground surface is necessary for the design of protective structures. Above-ground structures can be econom-

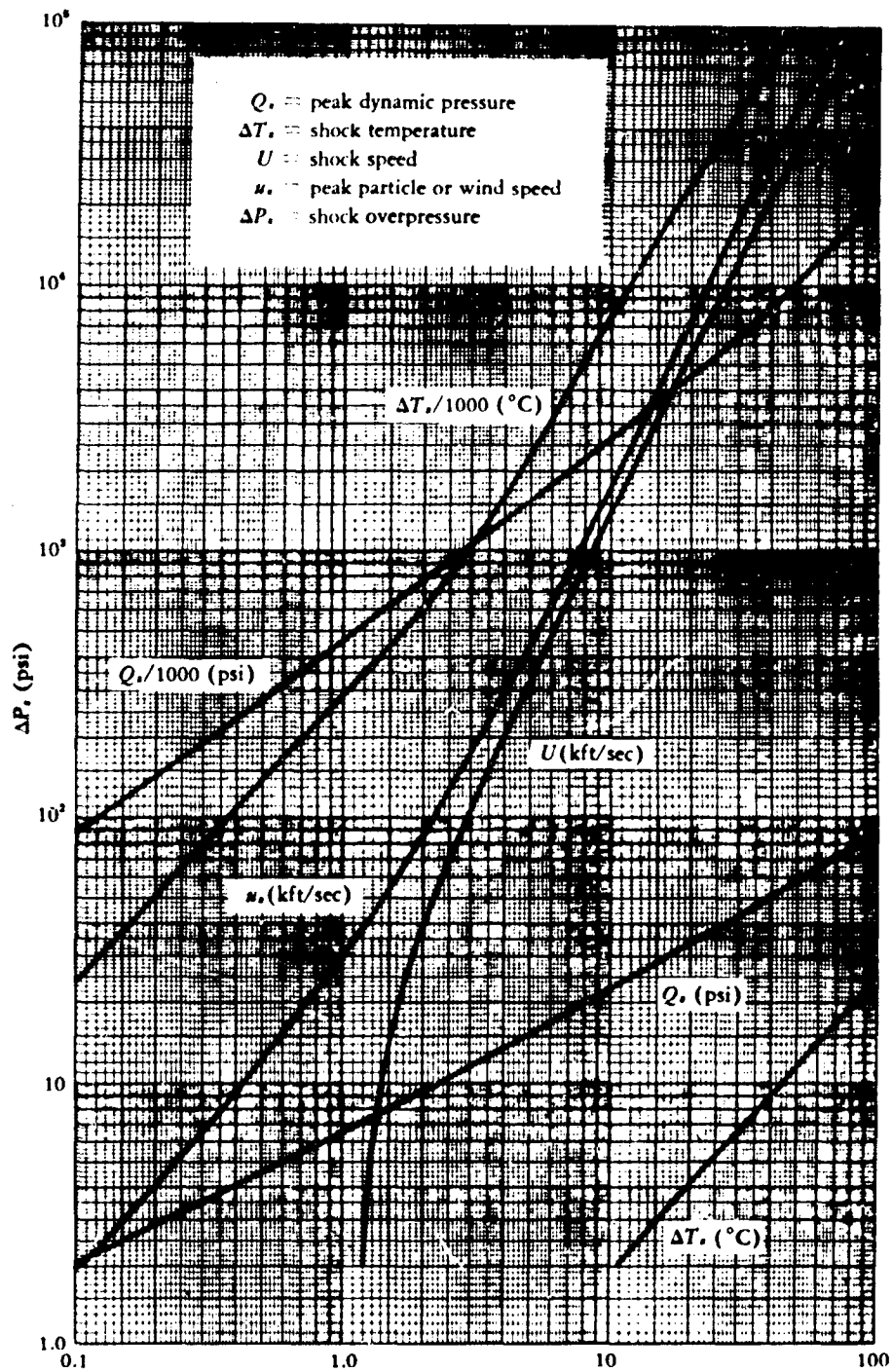


FIG. 29—Shock Parameters versus Shock Overpressure

ically designed to survive relatively low overpressures (even up to 50 psi), and surface conditions are therefore of great interest in such cases. Figure 31 shows the shock front after it has struck the ground beneath an air burst. A fused shock, called the "Mach stem," is formed

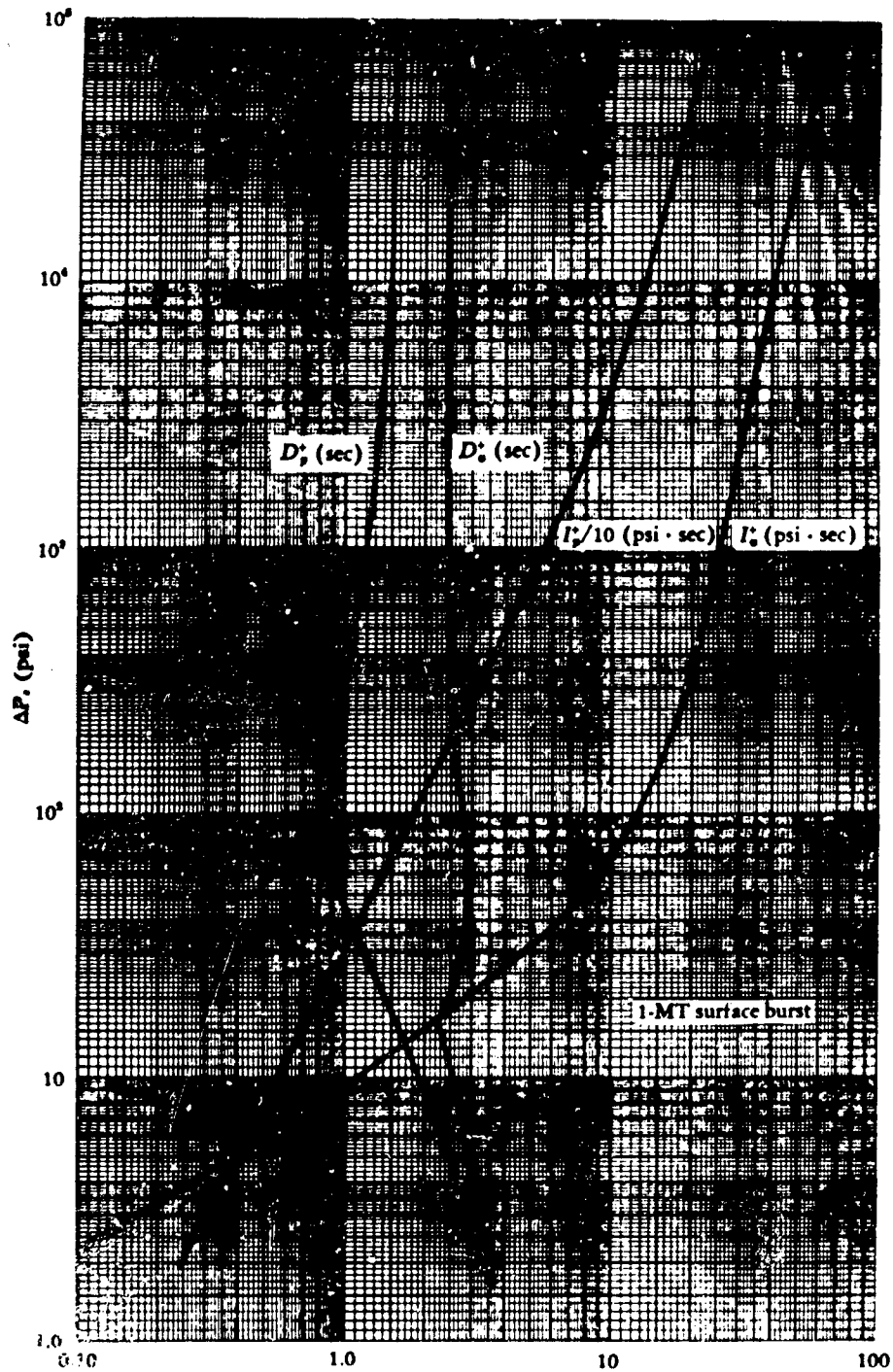


FIG. 30—Impulses and Durations for Overpressure and Dynamic Pressure for 1-MT Nuclear Surface Burst versus Peak Overpressure

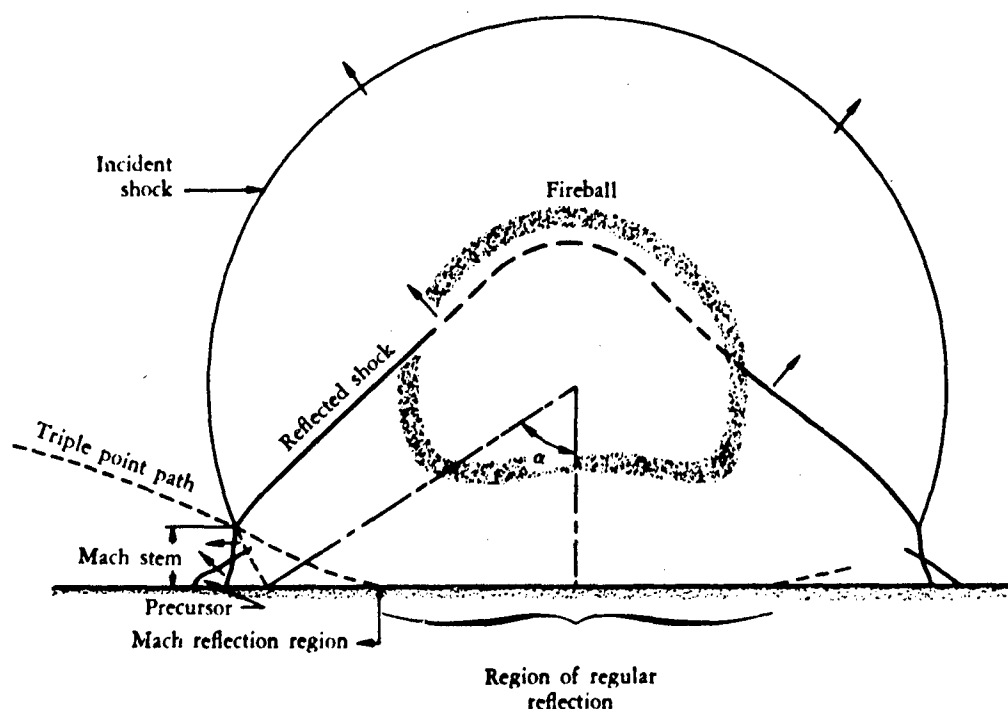


FIG. 31—Shock Configurations (Air Burst)

owing to the fact that the reflected shock front, traveling through a region previously heated by the incident shock, overtakes the incident shock front and merges with it. The merged shock, or Mach stem, then travels nearly parallel to the ground surface. In this region ( $\alpha \gtrsim 45$  deg), the fused shock is stronger for the same slant distance; and its height increases gradually as the shock expands. The region of regular reflection (where the incident shock is followed by a reflected shock but is not overrun by it) also leads to overpressures much greater than the incident overpressure. Figure 31 also indicates some distortion of the Mach stem and a precursor shock in front of it, both results of thermal radiation heating of the ground surface ahead of the shock. The pressure in such a precursed state does not have ideal properties but generally shows a slower rise to peak and a more irregular decay after maximum than are exhibited by normal shocks. For certain diffraction-type targets, such slow-rising pressures can greatly reduce the damage potential. For drag-type targets, the damage may actually increase because of precursed shock effects, since higher dynamic forces and greater irregularity in the duration and direction of destructive winds usually result.

When the shock front strikes an exposed surface normal to the shock ( $\alpha = 0$ ), the overpressure is raised almost instantaneously to a reflected overpressure. Normally reflected shock pressures can be calculated and are given in Fig. 32, which provides reflection factors versus

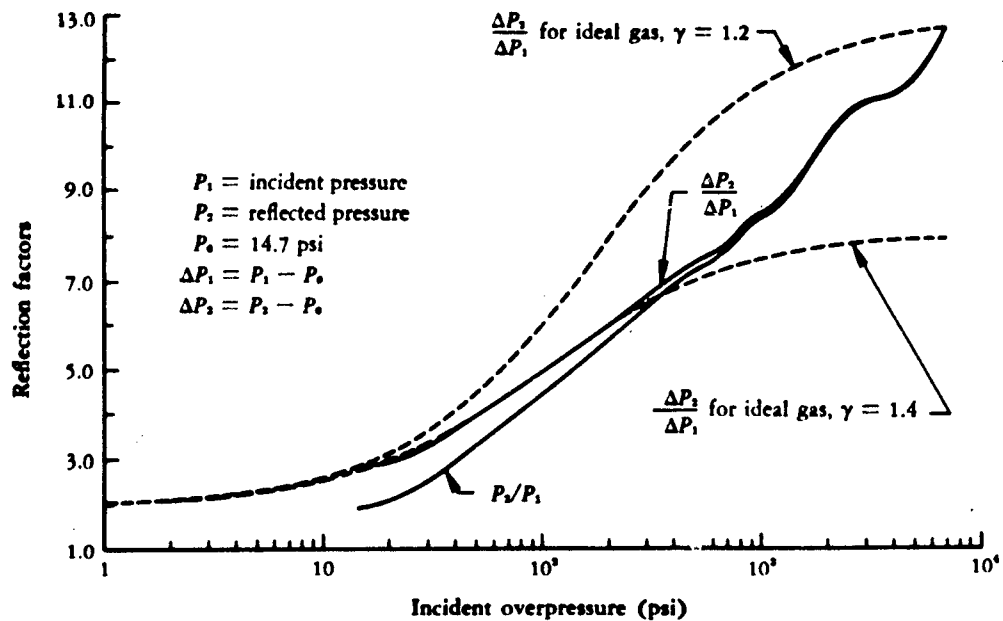


FIG. 32—Reflection Factors for Normal Shocks at Sea Level

initial peak overpressures. For shocks less than about 50 psi, an approximate ideal gas formula may be used to predict reflection factors:

$$R = \frac{\Delta P_r}{\Delta P_i} = 2 \left( \frac{7P_0 + 4\Delta P_i}{7P_0 + \Delta P_i} \right),$$

where  $P_0$  is the ambient atmospheric pressure. Figure 33 gives values of reflected overpressures as a function of angles of incidence of the shock front and of the incident overpressure up to 70 psi. These curves demonstrate a trend toward a simpler reflection with less Mach-stem enhancement at increasing overpressures.

For closed rectangular structures, it has been found by shock-tube tests that the reflected pressure ( $\Delta P_r$ ) is reduced to the stagnation pressure at a time after shock arrival about equal to  $3S/U$ , where  $S$  equals the height or half the width of the structure (whichever is less) and  $U$  is the shock speed. The time  $3S/U$  approximates the time required for the rarefaction waves, moving from the edges toward the center, to clear the front face of reflection effects.

The stagnation pressure is given by

$$P = \Delta P(t) + C_d Q(t),$$

where  $C_d$  is a drag coefficient and may be of the order of unity for the front face of a structure and  $Q(t)$  is the dynamic pressure given by  $\rho u^2/2$ , where  $\rho$  is the mass per unit volume of the shocked and compressed air and  $u$  is the free-stream velocity of the air particles in the

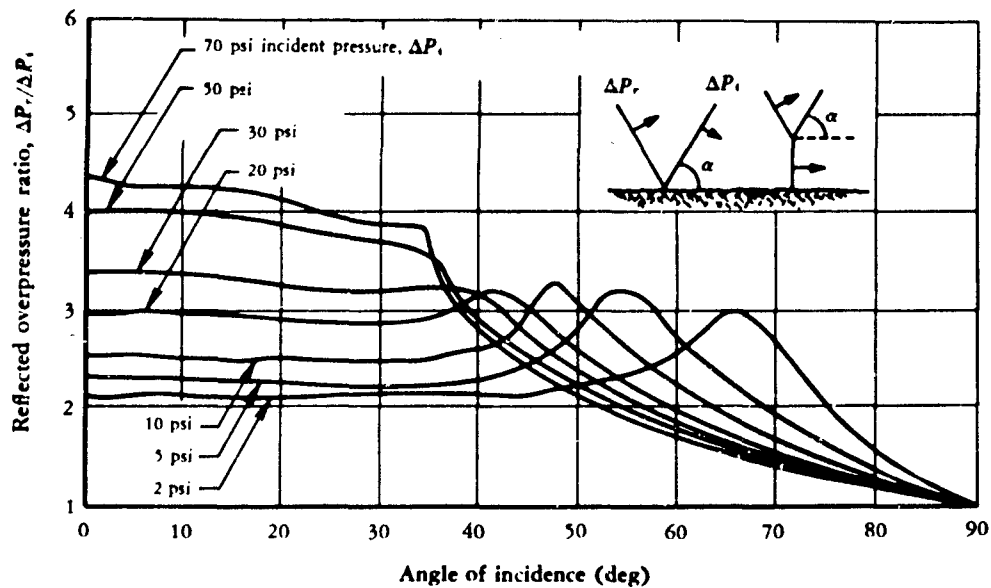


FIG. 33—Reflection Factors versus Incident Angle and Shock Strength

shock flow. For low overpressures, the maximum value of  $Q(t)$  is approximated by the equation

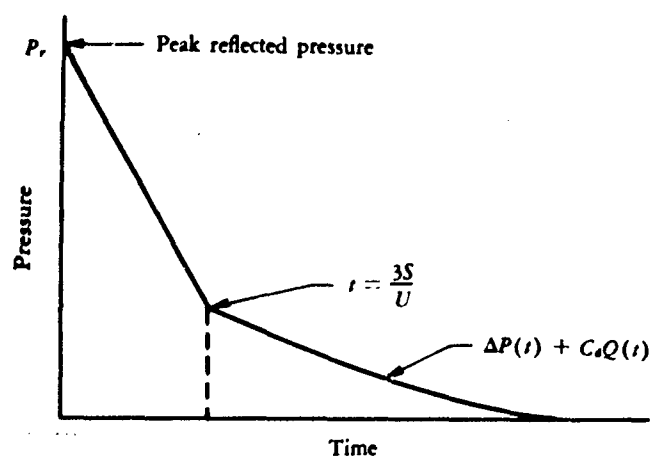
$$Q_s = \frac{\frac{5}{2} \Delta P_i^2}{7P_0 + \Delta P_i}$$

but a more generally valid value at all overpressures is given graphically in Fig. 29 (page 39).

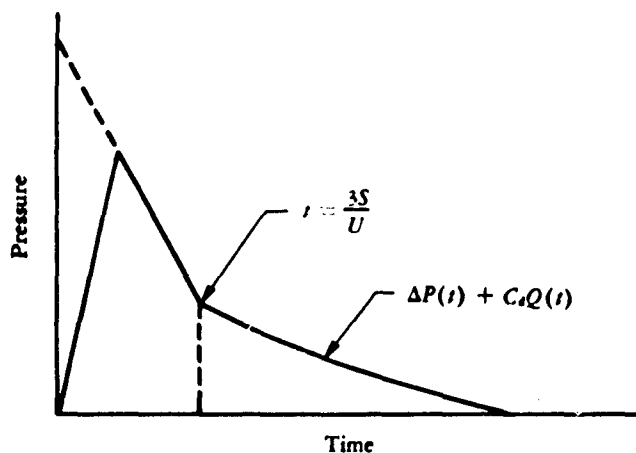
The nature of the average pressure versus time on a front face of a closed structure is suggested in Fig. 34 for both a fast- and a slow-rising applied load. Average peak pressures on the sides and top of a structure are obtained by taking the sum of the overpressure and the drag loading at the location  $L/2$  when the wave has traveled the distance  $L$ . (That is, the peak load corresponds to the overpressure and drag loading as defined by the time-dependent formulas at time  $L/2U$ ; but because the load is centered approximately at a distance  $L/2$  back from the front edge, it reaches a peak at time  $L/U$  after shock arrival.)

$$\frac{\text{Average load}}{\text{Area of top or side}} = \Delta P(L/2U) + C_d Q(L/2U).$$

The pressure on sides and top at any time is illustrated in Fig. 35. Similarly, pressures on the rear face are shown in Fig. 36. The approximate value of  $C_d$  for the side, top, and rear faces of a rectangular structure is  $-0.40$  for  $Q$  less than 25 psi, and  $-0.30$  for  $Q$  between 25 and 50 psi. The net horizontal loading on the closed rectangular structure is also shown in



(a) Fast-rise or ideal shock



(b) Slow or finite rise-time shock

FIG. 34—Average Front-face Pressure versus Time  
(Closed Rectangular Structure)

Fig. 36. Approximate blast loadings on more complex structural shapes such as domes and arches have been investigated and are covered in various engineering manuals.<sup>(3-6)</sup>

The preceding analysis of blast loading on simple structures corresponds closely to that provided in Ref. 1.

#### SHOCK PROPAGATION IN TUNNELS

Since any underground installation must have openings to the outside world for normal daily access, the influence of such openings on the vulnerability of the facility needs some

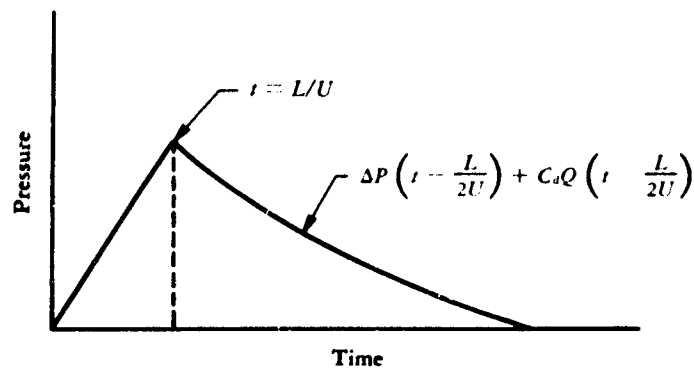


FIG. 35—Average Pressure on Sides or Top versus Time  
(Closed Rectangular Structure)

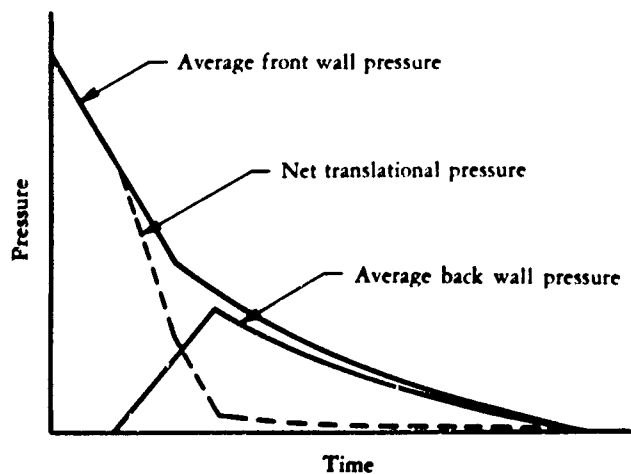


FIG. 36—Net Translational Pressure versus Time  
(Closed Rectangular Structure)

consideration. An opening into the crater of a large-yield surface explosion could not be counted on for useful exit or entry for a long period of time, since it would be collapsed, rubble-filled, and highly radioactive. An opening exposed to 1000 psi might be expected to survive. In any case an important question is: When an opening is exposed to pressures in the thousands of pounds per square inch, what kind of shock, at what strength, will travel down the tunnel and find its way into the interior?

Here the usual overpressure-versus-distance curve does not apply, since such a curve refers to a burst in the open air that decays rapidly both from the three-dimensional expansion into a rapidly increasing volume of air and from the shock heating of this air. A shock in a tunnel is quite analagous to the shock in a shock tube—a one-dimensional expansion for which the

rate of decay of the shock overpressure might be expected to be slower than in the open air. Even in a shock tube there is a certain amount of decay. There is some decrease as the shock is dissipated by heating the air in the tube, and further decay by losses to the walls through a boundary-layer formation. In addition, a shock wave with as rapid a time history as the entering air blast must drop in peak pressure because of the spreading of the pulse in time and space as it expands into a tunnel.

An approximate and intuitive expression for shock-wave attenuation in a tube might appear as follows:

$$\frac{\delta(\Delta P_s)}{\Delta P_s} = C \left( \frac{\Delta P_s}{P_0} \right)^n \left( \frac{L}{D} \right)^m \left( \frac{K}{D} \right)^l,$$

where  $\delta(\Delta P_s)$  is the change or decrease in shock overpressure in pounds per square inch,  $C$  is a "constant" of proportionality,  $\Delta P_s$  is the initial shock overpressure,  $P_0$  is the ambient pressure,  $L$  is the length of tube traversed,  $D$  is the diameter of the tube, and  $K$  is the equivalent wall-roughness dimension. The coefficients  $n$ ,  $m$ , and  $l$  are empirically determined positive exponents. Although crude, this equation indicates at least that attenuation is more rapid for stronger shocks; that it increases with tunnel length; and that it is also a function of the roughness of the tunnel walls. That is, for shock attenuation, long unlined or rough-walled tunnels would be preferable to short smooth-walled adits.

Even in a clean, smooth, hard-walled shock tube, the flow will become choked by the boundary-layer growth in a tube length of less than 500 diameters; as the shock progresses along the tube, a boundary layer grows behind it (as shown in Fig. 37), tending to choke off the laminar flow with turbulent flow. For example, for a 15-ft-diameter smooth-walled tunnel, this length for complete choking would correspond to  $1\frac{1}{2}$  mi. However, it is not necessary to go that far to get rid of serious shock effects, since 500 diameters represent a *limiting* distance for ideally smooth tunnels.

Some experimental evidence of the shock decay in a 4-in. shock tube is shown in Fig. 38. Here the smooth stainless-steel tube shows a reduction in shock pressure of a third in a length of 150 tube diameters—i.e., a pressure loss about proportional to the initial shock strength, indicating a value for the coefficient  $n$  of about unity for the pressure term in the previous approximate formula. Figure 39 shows a somewhat similar set of results using a 2-ft tube.

Another attenuating effect of equal importance is the decay of the peak shock overpressures because of the finite duration of the wave. After an explosive blast wave enters a tunnel, the driving pressure at the portal decreases exponentially with time. The finite nature of the blast pulse would attenuate the shock even if wall roughness did not. For example, in an ideal smooth-walled tunnel, the shock from a 10-MT burst would decay from a peak of

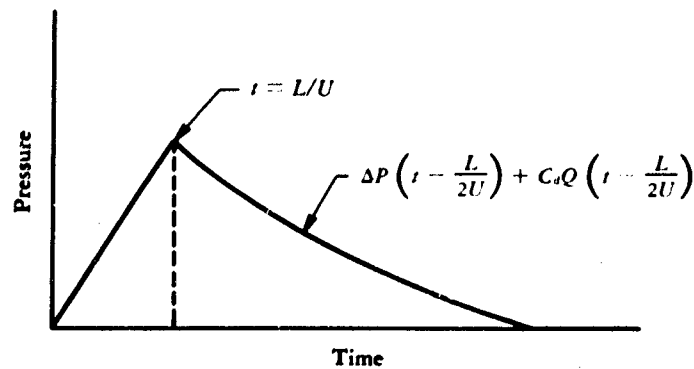


FIG. 35—Average Pressure on Sides or Top versus Time  
(Closed Rectangular Structure)

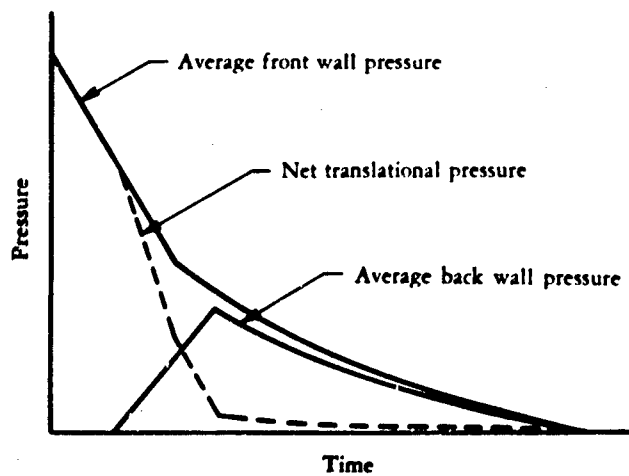


FIG. 36—Net Translational Pressure versus Time  
(Closed Rectangular Structure)

consideration. An opening into the crater of a large-yield surface explosion could not be counted on for useful exit or entry for a long period of time, since it would be collapsed, rubble-filled, and highly radioactive. An opening exposed to 1000 psi might be expected to survive. In any case an important question is: When an opening is exposed to pressures in the thousands of pounds per square inch, what kind of shock, at what strength, will travel down the tunnel and find its way into the interior?

Here the usual overpressure-versus-distance curve does not apply, since such a curve refers to a burst in the open air that decays rapidly both from the three-dimensional expansion into a rapidly increasing volume of air and from the shock heating of this air. A shock in a tunnel is quite analogous to the shock in a shock tube—a one-dimensional expansion for which the

rate of decay of the shock overpressure might be expected to be slower than in the open air. Even in a shock tube there is a certain amount of decay. There is some decrease as the shock is dissipated by heating the air in the tube, and further decay by losses to the walls through a boundary-layer formation. In addition, a shock wave with as rapid a time history as the entering air blast must drop in peak pressure because of the spreading of the pulse in time and space as it expands into a tunnel.

An approximate and intuitive expression for shock-wave attenuation in a tube might appear as follows:

$$\frac{\delta(\Delta P_s)}{\Delta P_s} = C \left( \frac{\Delta P_s}{P_0} \right)^n \left( \frac{L}{D} \right)^m \left( \frac{K}{D} \right)^l,$$

where  $\delta(\Delta P_s)$  is the change or decrease in shock overpressure in pounds per square inch,  $C$  is a "constant" of proportionality,  $\Delta P_s$  is the initial shock overpressure,  $P_0$  is the ambient pressure,  $L$  is the length of tube traversed,  $D$  is the diameter of the tube, and  $K$  is the equivalent wall-roughness dimension. The coefficients  $n$ ,  $m$ , and  $l$  are empirically determined positive exponents. Although crude, this equation indicates at least that attenuation is more rapid for stronger shocks; that it increases with tunnel length; and that it is also a function of the roughness of the tunnel walls. That is, for shock attenuation, long unlined or rough-walled tunnels would be preferable to short smooth-walled adits.

Even in a clean, smooth, hard-walled shock tube, the flow will become choked by the boundary-layer growth in a tube length of less than 500 diameters; as the shock progresses along the tube, a boundary layer grows behind it (as shown in Fig. 37), tending to choke off the laminar flow with turbulent flow. For example, for a 15-ft-diameter smooth-walled tunnel, this length for complete choking would correspond to  $1\frac{1}{2}$  mi. However, it is not necessary to go that far to get rid of serious shock effects, since 500 diameters represent a *limiting* distance for ideally smooth tunnels.

Some experimental evidence of the shock decay in a 4-in. shock tube is shown in Fig. 38. Here the smooth stainless-steel tube shows a reduction in shock pressure of a third in a length of 150 tube diameters—i.e., a pressure loss about proportional to the initial shock strength, indicating a value for the coefficient  $n$  of about unity for the pressure term in the previous approximate formula. Figure 39 shows a somewhat similar set of results using a 2-ft tube.

Another attenuating effect of equal importance is the decay of the peak shock overpressures because of the finite duration of the wave. After an explosive blast wave enters a tunnel, the driving pressure at the portal decreases exponentially with time. The finite nature of the blast pulse would attenuate the shock even if wall roughness did not. For example, in an ideal smooth-walled tunnel, the shock from a 10-MT burst would decay from a peak of

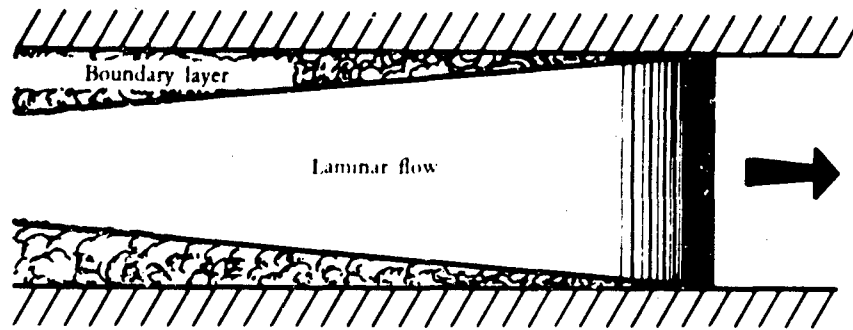


FIG. 37—Shock-tube Boundary Layer

$$\Delta P \approx \frac{2}{3} \Delta P_1 \text{ at } L/D = 150$$

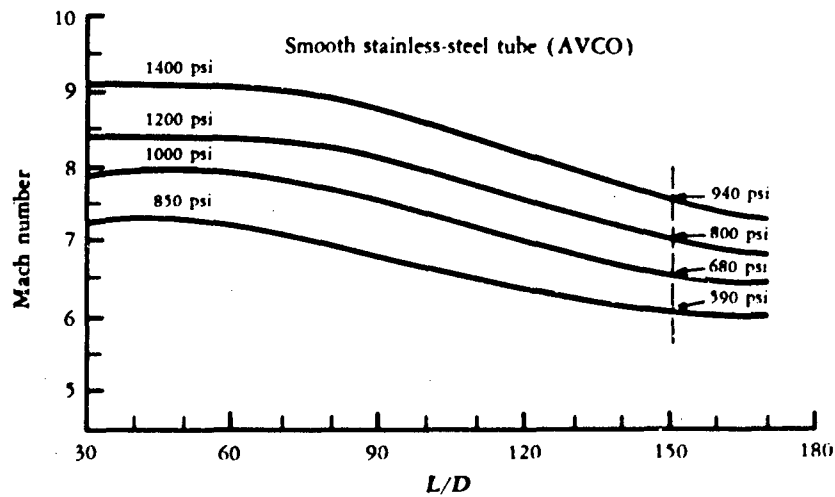


FIG. 38—Shock-tube Attenuation Data at High Overpressure

1000 psi at the portal to 100 psi at a distance substantially less than a mile down the tunnel. The combined influence of wall roughness and finite duration of the blast wave might be expected to reduce an entering shock by a factor of 10 (from 1000 psi to 100 psi) within a couple of thousand feet. For higher entering pressures, an even more rapid initial decay would be expected.

Doors or other shock-attenuating or -absorbing devices are necessary to shorten tunnel requirements and to ensure positive safety from air blast. A door at the portal is unattractive for at least two reasons: it must withstand the highest expected portal overpressures; and, if the portal itself is in the crater area, the door will be destroyed without fulfilling its mission. Mounting the doors well back in the tunnel protects them from the cratering action and sub-

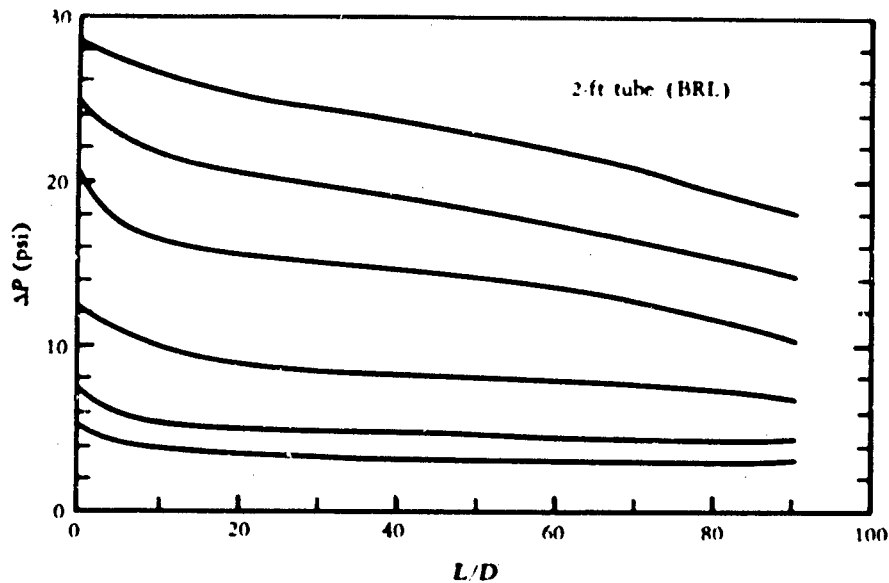


FIG. 39—Shock-tube Attenuation Data at Low Overpressure

jects them to somewhat lower overpressures. However, the reflected overpressures against a door blocking the tunnel would be considerably in excess of the incident tunnel shock. Following the normal reflection factors of Fig. 32 (page 42), a 3000-psi shock jumps to 33,000 psi, a 1000-psi shock rises to 8000 psi, and a 100-psi shock rises to 480 psi; a 10-psi shock, however, jumps to only 25 psi. In the confines of a tunnel such reflected pressures do not decay rapidly; they decrease at approximately the same rate as the initial pressure pulse until relief occurs at the portal and rarefactions can return to the point of reflection. These excessive reflection pressures can be minimized or avoided by any number of schemes. Various simple devices are suggested schematically in Fig. 40.

Perhaps the first thing that comes to mind in avoiding dead-end reflections is to arrange an entrance door so that it leads off from a continuing tunnel. This can most easily be done in connection with a double entrance, where the two (or more) entrances themselves may be separated far enough to avoid the possibility of both being destroyed by the same bomb explosion. Here an entering shock races by any inner tunnel door, exposing it or its corridors to the incident side-on pressure only—with no enhanced pressures from reflections, and with a considerable decrease at high incident pressures because of the reduction of dynamic pressures on turning the corner.

Various other schemes are feasible along a single tunnel, such as turning bends and corners, expanding into large chambers, or reverberating in a system of baffles and chambers

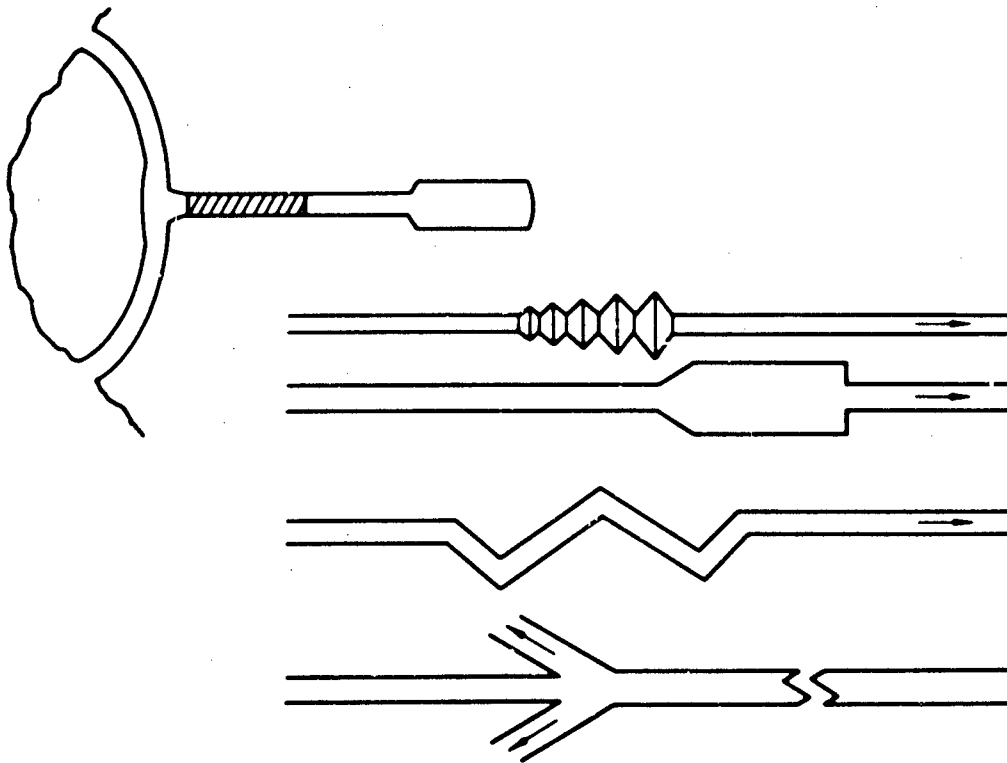


FIG. 40—Shock-attenuation Schemes

not unlike that employed for sound absorption. Side-tunnel results might be improved by branching off in the opposite direction from the incoming blast, allowing the shock to pass on down a long tunnel or into a large expansion and absorption chamber.

Any mechanical closure system has the disadvantages of possible jamming or malfunction after an explosion, of requiring detailed or awkward procedures for normal opening and closing, and of requiring considerable power in the movement of large masses. But the massiveness of a positive closure system is essential for absorbing the high impulses from nuclear blasts.

Much of the difficulty in moving large masses can be avoided by employing fluids. Opening and closing can be facilitated by filling and emptying a hollow door or the space between two bulkhead doors, using a liquid such as water. One step further, and *all* large moving parts could be avoided. If a sloping tunnel such as the one shown in Fig. 41 is used, gravity provides the bulkheads. Here only two water valves are needed: one to flood the tunnel and the other to drain it. If the location were one in which water was not plentiful, the water could be recirculated (as indicated), and only a small pump would be necessary to operate several openings and closings of the "water door" per day.

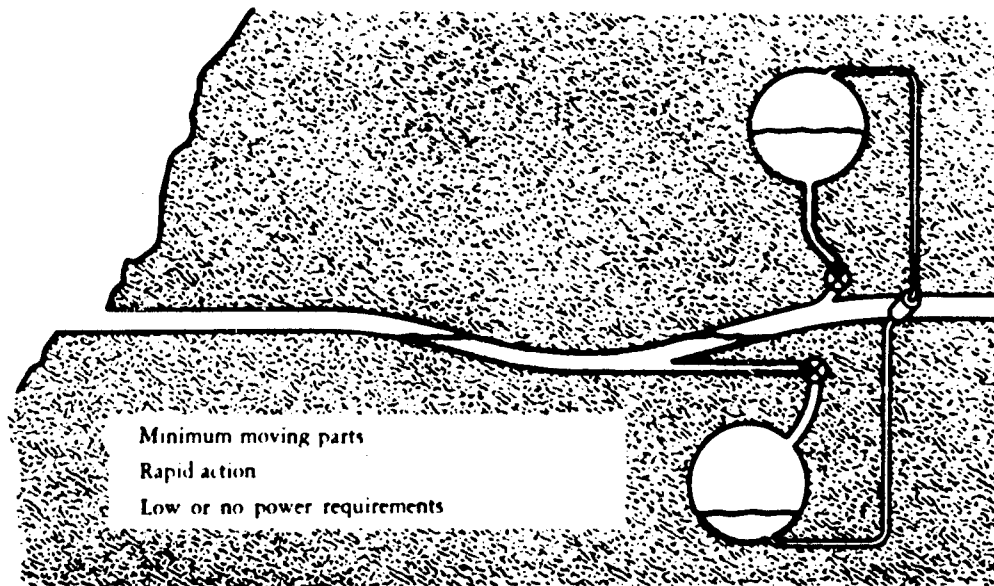


FIG. 41—Water Door

When blast strikes the surface of water—e.g., with 1000 psi—the pressure is both reflected and transmitted through the water, but it is not felt in the air beyond the water plug because of the poor impedance match. So long as the water has enough mass not to be accelerated to a high velocity by the pressure impulse, the transmitted pressure will be about 0.0003 of the incident pressure. Thus, 1000 psi incident pressure reflects to 8000 psi and transmits as  $0.0003 \times 8000$ , or 2.4 psi. But, in order not to drive the water down the tunnel at high speed, something on the order of 100 ft of flooded tunnel is needed. For an example, consider a 10-MT burst and 1000-psi pressure at the tunnel entrance. If a water door is then situated inside the tunnel at a point where the incident pressure will be 150 psi, the total impulse in the reflected pressure on the water surface will be about 200 psi · sec. A plug of water only 10 ft thick would make quite a splash, with velocities on the order of 1400 ft/sec; but with 100 ft of water, more appropriate for the sloping-tunnel notion, initial water velocities of a tenth of that (140 ft/sec) would result and could be easily dissipated by splash barriers, diverted down side tunnels into reservoirs, or allowed to fall through a grating in the tunnel floor into the recirculating reservoir. The advantages of various such fluid-filled closures stem from their simplicity and reliability—the possibility of fairly rapid closing (and opening) with low energy requirements, minimal moving parts, and no heavy machinery.

## VIII. AIR-BLAST-INDUCED GROUND SHOCK

A SHALLOW-BURIED STRUCTURE may be made quite safe from nuclear and thermal radiations and from the direct effects of air blast, so that the primary remaining vulnerability may be associated with the violent movements of the surrounding earth.

In addition to the intense direct shock in the ground that is responsible for the crater formation, ground motions are induced by the passage of air blast over the surface. For most surface or shallow-buried structures, this air-induced ground shock is of great significance since it is extended to large distances by the air blast, while the direct ground shock is more rapidly attenuated below damaging levels in passing through the intervening earth mass.

As long as the shock wave in air is strong and is moving at very high speed, the shock induced in the ground can only trail behind and below the air shock. In such a case, the ground shock can be conveniently characterized by the intensity and duration of the air blast passing nearly directly above. As the air shock slows and moves at speeds approaching the speed of sound in undisturbed air, the shocks generated in the ground may disperse because of their higher speeds (seismic speeds in soil or rock are generally several times faster than sound speed in air), and so may move ahead as well as below and behind the air-shock position. The wave histories in this latter case are generally more complex and show greater variation from soil inhomogeneities and stratifications.

The acceleration-versus-time traces in Fig. 42 perhaps overemphasize the irregular and unpredictable nature of the ground shock in this outrunning phase. Note that some signal is felt prior to the arrival of the shock directly above the station ( $t = 0$ ). Note also that the maximum acceleration occurs well after shock arrival. One can at least derive some reassurance from the fact that the peak acceleration is less at depth and that some of the sharpness or higher-frequency components are missing at greater depths. This aspect points to a weakness in the applicability of elastic wave propagation theory. Dissipative mechanisms, either natural or artificial, can be extremely effective in reducing the peak stress or maximum velocity from such highly transient loads as those from air blast.

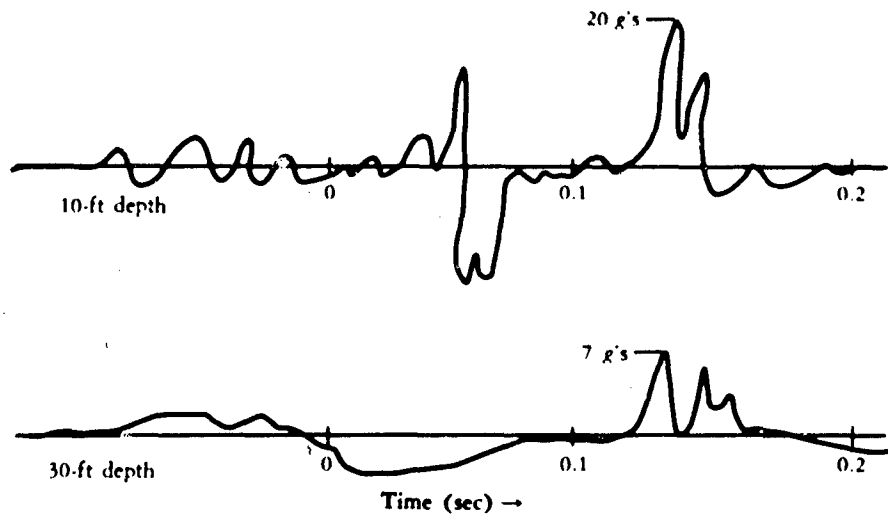


FIG. 42—Vertical Accelerations at Shallow Depths

Unfortunately, there is no entirely satisfactory method of extrapolating the meager test results to other soil types or other burst positions or yields. Theoretical efforts are not yet sufficiently sophisticated to provide the physical interpretation necessary for such extensions, so that at present more direct empirical correlations are more useful. A set of approximate formulas of this kind are provided by F. M. Sauer<sup>(7,8)</sup> for peak values of acceleration, velocity, and displacement near the surface. These formulas, given below, differ for the situations where the air shock is superseismic (i.e., faster than the seismic velocities in the soil) and where the ground shock can arrive before the air shock (identified as "outrunning" by Sauer).

#### SUPERSEISMIC GROUND-SHOCK MAXIMA (AT 5-FT DEPTH)

*Vertical acceleration:*  $\alpha_{vm} \approx 340\Delta P_s / C_L \pm 30$  per cent. Here acceleration is measured in  $g$ 's and overpressure ( $\Delta P_s$ ) in pounds per square inch. An empirical refinement requires  $C_L$  to be defined as the seismic velocity (in feet per second) for rock, but as three-fourths of the seismic velocity for soil.

*Vertical velocity:*  $u_{vm} \approx 75\Delta P_s / SC_L$  ft/sec  $\pm 20$  per cent. The specific gravity of the earth medium is denoted as  $S$ . In the following, the overpressure impulse (positive phase only) is designated as  $I_p$ .

*Vertical displacement:*  $d_{vm} \approx 20I_p (\Delta P_s)^{1/2} / SC_L$  ft  $\pm 30$  per cent. Since no attenuation is presumed, the stress is taken to be the same as the loading overpressure, but an exponential decay (as suggested earlier) may be more reliable.

*Vertical strain:*  $\epsilon_{vm} \sim 1.1 \times 10^5 \Delta P_s / SC_L^2$  parts per thousand  $\pm 30$  per cent. Values of maximum *horizontal* displacement are likely to be half (or less) of the vertical maxima, while maximum horizontal acceleration and velocity are expected to be more nearly comparable to the vertical maximum values.

#### OUTRUNNING GROUND-SHOCK MAXIMA (AT $\sim 10$ -FT DEPTH)

*Vertical acceleration:*  $\alpha_{vm} \approx 2 \times 10^5 / C_L r^2$   $\pm$  factor of 2. Acceleration is measured in  $g$ 's, and  $r$  is the scaled radial distance—i.e.,  $r = R/W^{1/3}$  kft/(MT)<sup>1/3</sup>.

*Vertical velocity:*  $u_{vm} \approx 4 \times 10^5 / SC_L r^2$  ft/sec  $\pm 50$  per cent.

*Vertical displacement:*  $d_{vm} \approx 6 \times 10^4 W^{1/3} / SC_L r^2$  ft. Horizontal motions in this outrunning phase may be quite comparable to the vertical movements.

Using these formulas in two examples may help to establish their limited usefulness. Consider a soil with a seismic velocity of 4000 ft/sec (thus,  $C_L = 3000$ ), and introduce a ground shock from an air-blast load of peak overpressure equal to 500 psi. The air-shock speed for this overpressure (see Fig. 29 on page 39) is faster than this seismic velocity above  $\sim 400$  psi, so one should refer to the superseismic relations, which for this level give a maximum vertical acceleration of 57  $g$ 's, with an uncertainty of 30 per cent—allowing the expected value to be anywhere between 40 and 74  $g$ 's.

If this soil has a specific gravity of about two, then the peak vertical velocity predicted for this 500-psi load is about 6.25 ft/sec, or between 5 and 7.5 ft/sec.

For a 1-MT surface burst, and again at the 500-psi point, the overpressure impulse is about 40 psi·sec, so that for this same soil example the displacement is estimated to be between 5 and 10 in., with a best value being 7.5 in.

In the outrunning region, consider the same soil and a 1-MT surface burst at the 100-psi point. Since the shock radius at the 100-psi point for 1 MT is about 3500 ft, the reduced radial parameter in these formulas becomes 3.5. The predicted acceleration at this range is about 5  $g$ 's, with a range from 2 to 20  $g$ 's equally possible. Such wide ranges stem largely from the complexities imposed on the ground motions by the signals refracting or reflecting from other surface points and from possible layered strata in the ground. In this outrunning phase, such signals can overtake, and indeed overpower, the motions stemming more directly from the overhead blast load at any instant.

Following the same example at 100 psi, the expected maximum velocity lies between 3 and 9 ft/sec, with a mean prediction of 5.4 ft/sec. Similarly, the expected maximum displacement for this case is 10 in.; but here, as is the case with the rest of these semi-empirical

formulas, there is need for caution. These expressions are inapplicable when extrapolated into regions of overpressure, weapon yield, or type of soil or rock much outside the realm of our test experience.

#### ATTENUATION WITH DEPTH

Data taken on a low air-burst shot in Nevada indicate an exponential decay of maximum displacement with depth. For the particular case of a burst of  $\sim 40$  KT at 700 ft, some measurements were made as deep as 200 ft below the surface of Frenchman Flat (a dry lake bed), which led to the following approximate decay law, according to Perret:<sup>(1)</sup>

$$\delta = \delta_0 \exp(-0.017D),$$

where  $\delta$  represents the maximum vertical displacement induced at depth  $D$ ,  $\delta_0$  is the maximum displacement at the surface, and  $D$  is the depth in feet.

Estimates of maxima at great depths can be made by accounting for attenuation by means such as those suggested by Perret. However, care should be used to distinguish the attenuation due to geometry from that due to dissipative mechanisms in the soil dynamics. The latter will depend primarily on the travel path of the earth shock and on the dominant periods or frequencies in the wave. Since the period of the blast load changes quite slowly with explosion yield, the dissipative attenuation for a given depth and given peak overpressure level will not be a sensitive function of the yield except at very great depths or very high overpressure levels. This dispersion does reduce the peak stress by smearing the wave fronts and causing longer rise times to peak stress, which often means more uniform loading of buried structures.

In some contrast, the effect of geometry may be negligible for shallow-buried structures subject to loading by large yields but may be very pronounced for comparable loading from small-yield explosions. To illustrate this geometry, Fig. 43 shows the wave fronts in the air-induced ground shock. In the examples used, the earth media have seismic velocities of 2500 and 5000 ft/sec, and fronts are shown at times when the peak air overpressures are 10,000, 1000, 300, and 100 psi. The curves represent positions achieved at uniform seismic velocities and take no account of faster ground-shock propagation at the highest stress levels or of variations in seismic velocity with depth. It is interesting to note that the effect of the rapid slowing of the air shock at around 300 psi (where it approaches the 5000-ft/sec seismic speed) results in a steepening of the wave front and in a piling-up of the signal or waves from a considerable range of earlier shock positions. A similar condition is beginning at 100 psi for the slower seismic speed case (2500 ft/sec), but it is less pronounced since the air-shock speed is decreasing more gradually and so permits less of the ground wave to be superimposed. For

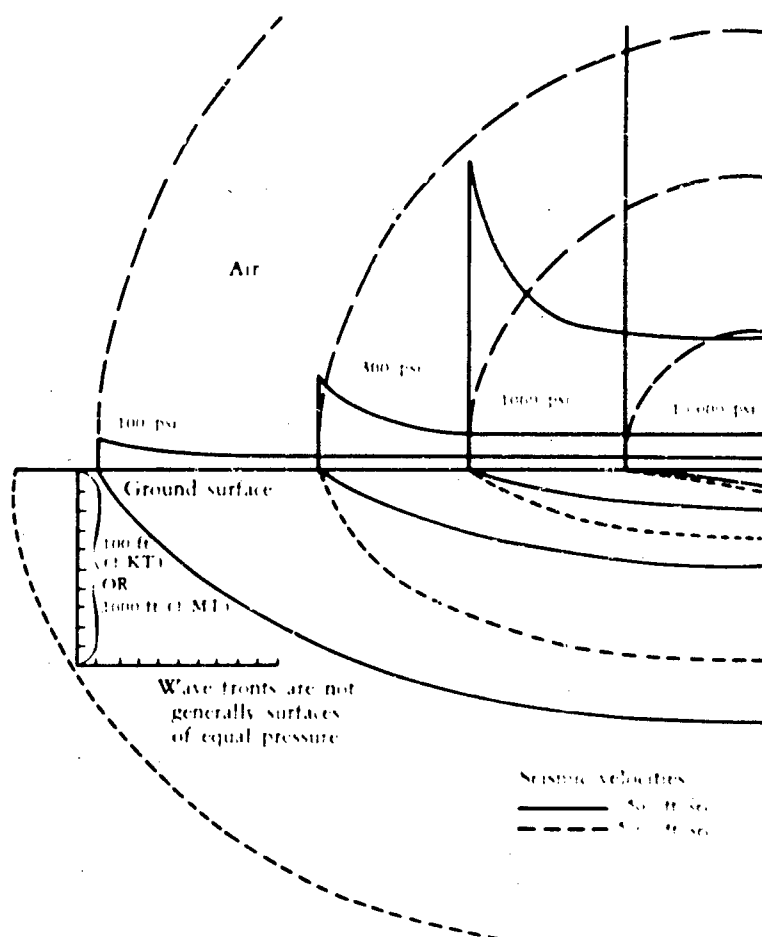


FIG. 43—Air-shock-induced Ground Motion Wave Fronts for Peak Overpressures of 10,000, 1000, 300, and 100 psi, and for Seismic Velocities of 2500 ft/sec and 5000 ft/sec

the case of a 5000-ft/sec seismic velocity soil and an air shock at 100 psi (therefore traveling at less than 3000 ft/sec) clearly some signal in the soil can propagate ahead of the air shock, thus representing a region where one must expect ground-shock signals to arrive even before the air-blast arrival (the "outrunning" phase previously described).

It is obvious, but worth further emphasis, that the wave fronts of Fig. 43 do *not* represent surfaces of equal pressure. In fact, the lack of spherical divergence in the wave front directly below the point of burst would suggest that less geometric attenuation will occur there than in a more symmetric explosion. In the same vein, the ground shock just below the shock front at the 300-psi point for the 5000-ft/sec seismic speed case includes signals from pressures considerably higher than 300 psi and could, in that region, show ground stresses higher than the air overpressure.

It is equally certain that as we go to greater depths or to smaller yields—they are the same thing since both depth and distance scale with the cube root of the yield—the spherical divergence of the shock energy into the below-ground space must further attenuate the shock strength.

For the lower overpressures when the ground-shock wave fronts are not seriously distorted by the air-shock speed—i.e., beyond the early superseismic stage shown in Fig. 43—the geometric stress attenuation can be approximated from the formula proposed by Newmark:<sup>(6)</sup>

$$\begin{aligned}\sigma_{vm} &= \alpha_z \Delta P_s, \\ \alpha_z &= \frac{1}{(1 + Z)/L_w}, \\ L_w &= \frac{2300W^{1/3}}{(\Delta P_s)^{1/2}} \text{ ft},\end{aligned}$$

where  $\Delta P_s$  is the peak overpressure at the surface (in pounds per square inch),  $\sigma_{vm}$  is the maximum stress (in pounds per square inch) at depth  $Z$  (in feet),  $\alpha_z$  is the geometric attenuation factor, and  $W$  is the yield (in megatons). This expression is plotted for ready reference in Fig. 44.

The approximation is based on a pseudostatic load model with some semi-empirical correction for the higher air-shock velocities. The use of this formula or of Fig. 44 cannot be recommended in much of the region illustrated in Fig. 43, since the basis of the approximation views the load as static and/or the seismic velocity as infinite. This view does not permit the existence of stresses anywhere higher than that in the shock front at that instant—a condition that can apply only when the shock speed is truly low compared with the seismic speed.

### SHOCK SPECTRA

In designing for shock isolation, some information on the frequency characteristics of the ground shock is helpful, although for thorough analysis nothing short of full time histories of the expected motions can be adequate. At high frequencies (greater than  $\sim 100$  cycles per second, or cps), the acceleration limits are most significant, since neither large amplitudes nor high velocities are likely to occur when the motions are reversing hundreds of times per second. At the lowest frequencies, the displacements are of greatest concern. At fractions of a cycle per second (frequencies typical of earthquakes), the displacements can become a matter of several feet while accelerations remain less than one and velocities are low. For such displacements, it is important to provide rattle space, or adequate room for isolated or shock-mounted equipment to swing without colliding with walls and unmounted equipment. Secondary missiles set

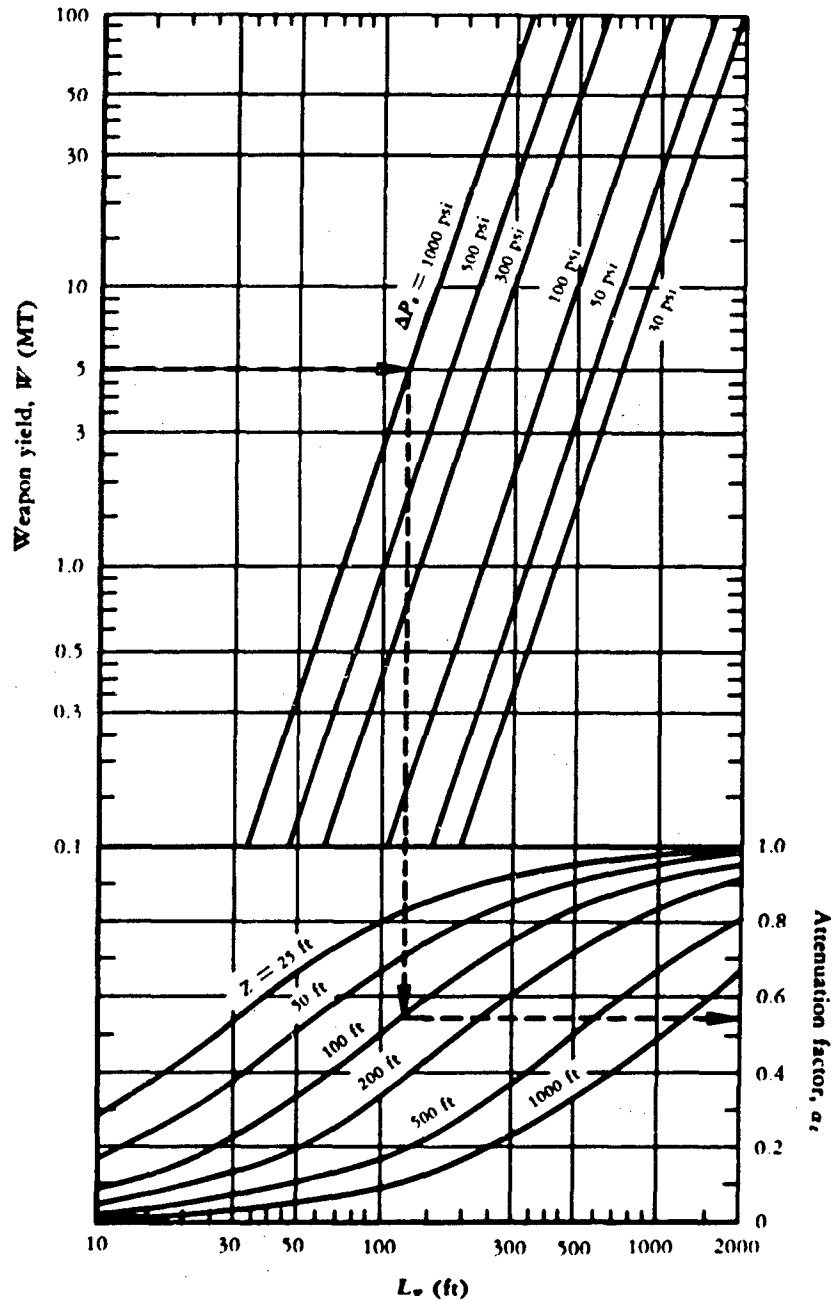


FIG. 44—Geometric Attenuation with Depth

in motion by the acceleration of the basic structure can be minimized by thorough tie-down procedures and careful housekeeping.

As it happens, a convenient form in which to express the expected shock-spectra input to a structure is on a harmonic plot that specifies a fixed peak acceleration above 100 cps, a peak velocity between 1 and 100 cps, and a maximum displacement below 1 cps. The test data

only approximately follow this simplified pattern. Because of the harmonic nature of elastic wave propagation, a logarithmic plot combining acceleration, velocity, and displacement limits is possible. Such a plot for the vertical ground-shock spectra, showing some arbitrary limits for 100 psi and 500 psi for a soil having fairly representative properties, is given in Fig. 45. These limits are intentionally high to represent expected extremes and to cover uncertainties in extending the test data.

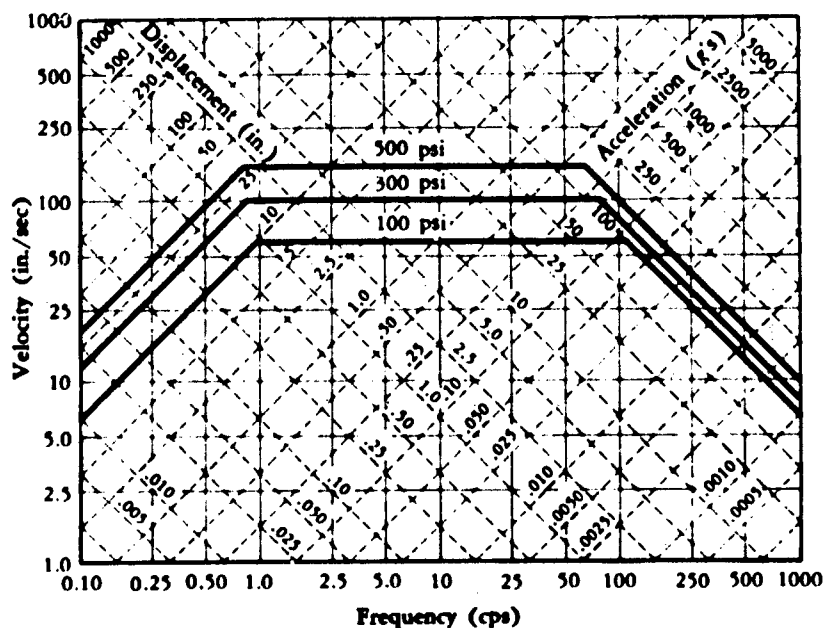


FIG. 45—Vertical Shock Spectra

As with the analysis of the response of structures to air blast, the response of buried structures to ground-shock motions is a complex function of the structure's interaction with the load as it varies in both space and time. There can in general be reflections and diffraction effects, so that the free-field phenomenological descriptions of the ground motion (as partially provided here) represent only a first step in the determination of structure and contents response.

## IX. DEBRIS AND FALLOUT

HAVING SURVIVED A NEAR MISS in a protected installation, one might ask the question: What else can happen and how soon will it be over? Immediately following the blast-wave positive phase, a negative phase sets in, in which the winds reverse to blow toward ground zero, and the overpressure becomes an underpressure (less than ambient). This negative overpressure can approach as much as 3 psi of suction, which could exert considerable lift on a sealed, pressurized installation. (A 3-psi partial vacuum could lift a concrete lid 3 ft thick!) The reversed winds may be strong enough to bring back some debris to clog openings or revetments. These winds do not stop within a few seconds, but fade into the circulation set up by the rising fireball. The late fireball is still hot but at nearly normal pressure, so that its interior is at low density—forming a kind of buoyant balloon in the atmosphere. Figure 46 shows the densities versus radius at times as late as a few seconds. This several-thousand-foot-diameter, low-

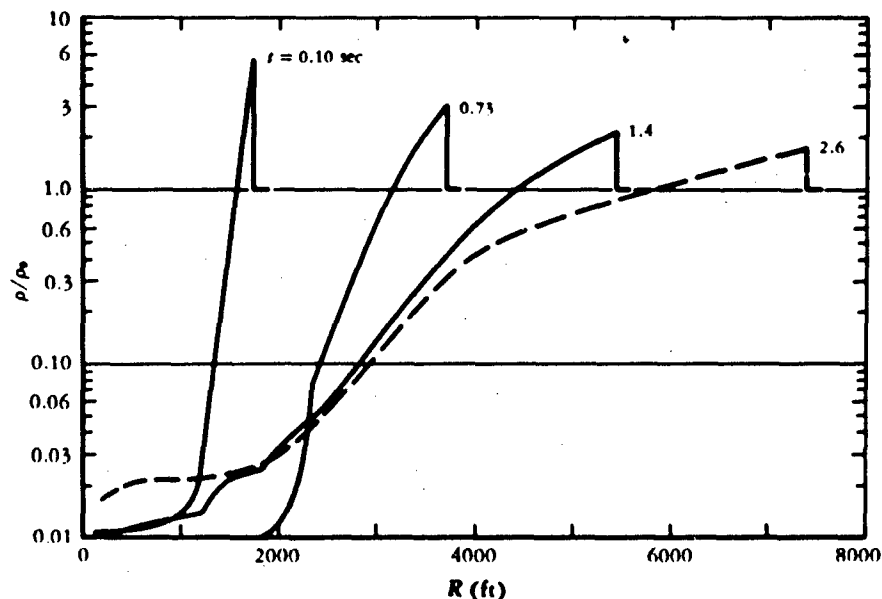


FIG. 46—Late Fireball Densities (1-MT Surface Burst)

density sphere begins immediately to rise as a bubble as the denser air around it forces it upward. The rate of rise after a few seconds approaches 400 ft/sec. The circulation is such that the air velocities in the dust-laden stem that flows up through the rising cloud (Fig. 47) are about twice the cloud-rise velocities, or as much as 800 ft/sec. The consequences of such wind velocities can be better appreciated when it is considered that the drag created by this flow could hold aloft a boulder weighing as much as 7 tons or could loft lesser rocks and debris to very high altitudes. The cloud continues to rise for 4 to 6 min, which can take it to altitudes over 60,000 ft, depending on meteorological conditions. Even after the cloud has stabilized, the stem continues to rise as the circulation persists. During the time of the initial cloud rise, much of the cratered debris is aloft on various trajectories. Much of this material will be excavated at pressures below that needed to pulverize or vaporize the rock or soil, and some of it will be lofted in essentially its original sizes and shapes. If the soil is rocky, or if concrete and steel structures are involved, some large fragments must be expected at ranges at least as large as the stem radius; and there is some chance that rocks may rain down over a wide area for many minutes after a burst.

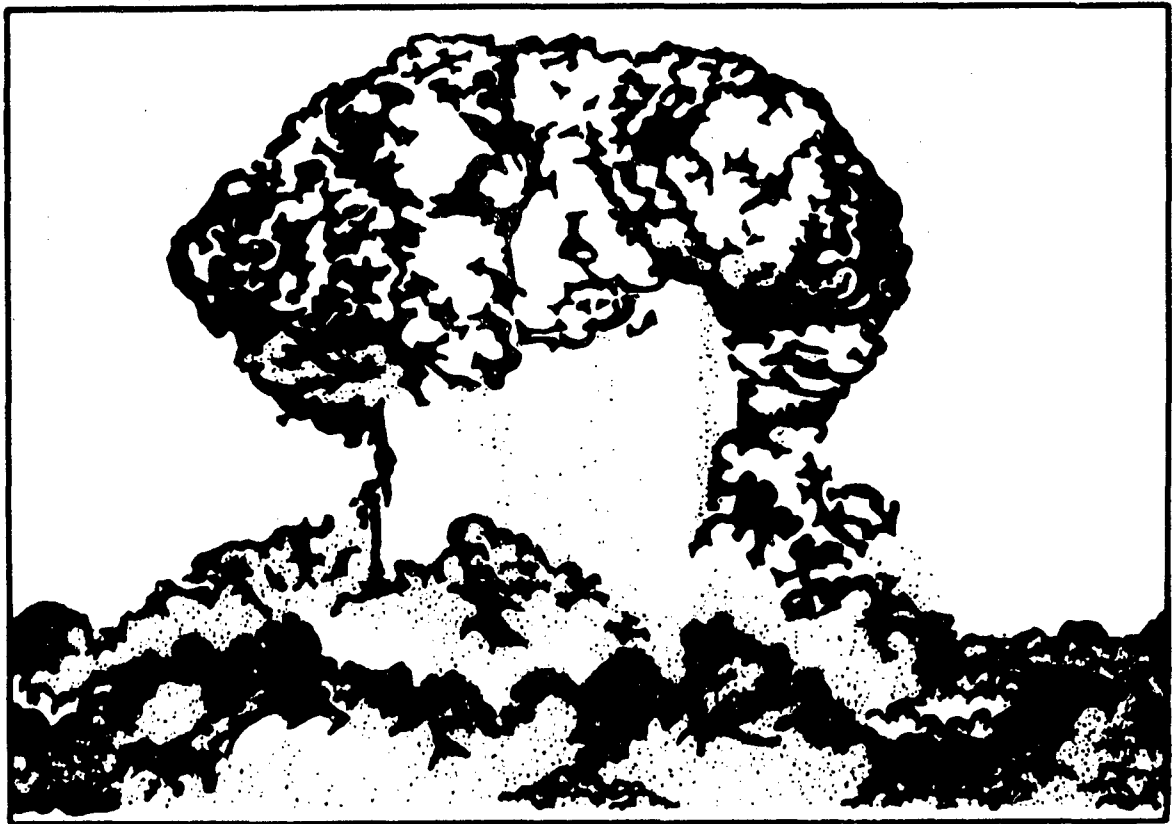


FIG. 47—Late Fireball Turbulence

Again, if the wind circulation closely corresponds to the visible cloud and stem movements, wind velocities of the same order of magnitude ( $\sim 100$  ft/sec) may be expected at the base of the stem—i.e., in the dust-laden air above shelter.

Visibility will be restricted and unpredictable over an area corresponding to at least the 10-psi distance from such bursts, so that visual assessment of the post-burst external environment will not always be possible. Direct human exposure would be undesirable, possibly even fatal, in the local fallout, which outside the immediate crater area (but within 10 mi or so) can rise to thousands of roentgens per hour in the first hour, falling to a few hundred at the end of a day. Total doses (integrated over time) after 18 hr may be in excess of 3000 roentgens over 1000 sq mi. Clearly, surviving nearby surface installations or support structures will not be habitable for many hours after a megaton-weapon surface burst, even in extreme emergencies. The extent and intensity of fallout depend critically on weapon design, details of burst position, and properties of soil and surrounding material. Although it is possible by design to enhance the radioactivity produced within a weapon, the height or depth of burst is more influential, and the nature of the cratered material is as important.

Slight burial can increase the intensity (while reducing the area coverage) of downwind fallout by several fold over that from a surface burst, while even slight elevation above the surface can reduce manyfold the intensity (and area coverage) of local fallout. Most of these uncertainties are not reflected in fallout predictions, nor do such predictions consider the fact that higher-yield surface bursts are expected to excavate and carry aloft a mass or volume of earth less than proportional to the explosive yield. The radioactivity produced is roughly proportional to the fission fraction of the explosion yield, but the amount brought down in local or downwind fallout is determined by the scavenging action of cratered material. Crater volumes increase less rapidly than linearly with increasing yields. The amount of debris available to bring to earth the vaporized atoms of the fission-fragments is proportionately less for larger yields—particularly if the bursts are on or above the earth's surface.

## X. FIRES

FIRES have long played a major role in the destruction of wartime targets, yet much about the subject remains poorly understood. The concern here is limited to the influence that fires may have on the design of protective structures. It is clear that protection from fire effects is a necessary part of some shelter designs, but it is equally clear that once protection is provided against the destructive effects of blast and direct radiations, the hazards from fire are reduced.

Both the incidence and the consequence of fires become more serious in the presence of other destructive forces. Earthquakes, violent storms, or disruption by war can lower fire-fighting effectiveness and allow fire to spread. Uncontrolled spread is most certain when extensive physical damage (e.g., from blast or earthquake) accompanies the ignition of many separate fires. The blast disruption itself may provide many secondary fire sources and may expose much combustible matter that otherwise might resist ignition.

Some fire-related factors pertinent to sheltered persons are the following:

1. Although blast-resistant structures usually provide an adequate measure of protection, shielding from heat radiation and flames from nearby burning structures should be considered a part of design requirements.
2. Provision for excluding external air during conflagrations can make it unnecessary to monitor and filter intake air for smoke and dangerous concentrations of noxious gases such as CO or CO<sub>2</sub>. Positive closure, or maintenance of slight excess internal pressure from stored air sources, can be most effective and need not operate for more than a few hours.
3. Although fire-gutting of structures seldom lasts for more than 1 or 2 hr, hot rubble and smoldering remains can continue to be a minor hazard for periods of days; they are likely to be serious, however, only if they accumulate on shelter exits or air intakes. Such contingencies are, in principle, easy to avoid.
4. Fire consequences can be greatly ameliorated by protective and preventive efforts *prior to attack*. Removal of combustible stores from the vicinity of shelter exits and

entrances, elimination or covering of materials particularly susceptible to thermal ignition, the use of noncombustibles in nearby construction—these precautions can be helpful, particularly where high thermal input is not accompanied by intensive blast.

## REFERENCES

1. GLASSTONE, SAMUEL (ed.), *The Effects of Nuclear Weapons*, rev. ed., U.S. Department of Defense, U.S. Atomic Energy Commission, April, 1962.
2. NATIONAL ACADEMY OF SCIENCES, *Future Weapons and Weapon Effects*, Project HARBOR (Group B), September, 1963.
3. AMERICAN SOCIETY OF CIVIL ENGINEERS, *Design of Structures To Resist Nuclear Weapon Effects*, ASCE Manual of Engineering Practice No. 42, American Society of Civil Engineers, New York, 1961.
4. MELIN, J. W., AND A. P. ROBINSON, *The Analysis of the Dynamic Response of an Above-ground Simply Supported Cylindrical Shell Subjected to Blast Loading*, Air Force Special Weapons Center, AFSWC-TR-61-55, August, 1961.
5. HUANG, T., S. IYENGAR; AND R. L. JENNINGS, *Studies of Response of Arches and Domes under Dynamic Loads*, Air Force Special Weapons Center, AFSWC-TR-61-90, October, 1961.
6. NEWMARK, N. M., AND J. D. HALTIWANGER, *Principles and Practices for Design of Hardened Structures*, Air Force Special Weapons Center, AFSWC-TDR-62-138, December, 1962.
7. SAUER, F. M., "Ground Motion from Above-ground Nuclear Explosions," Chapter IV-1 in *Nuclear Geoplosics*, Defense Atomic Support Agency, DASA-1285, May, 1964.
8. ———, "The Nature of Ground Shock Induced by Airblast from Above-ground Nuclear Explosions," in *Proceedings of the Symposium on Scientific Problems of Protective Construction at the Swiss Federal Institute of Technology*, July 25-30, 1963, Bundesamt für Zivilschute, Berne, Switzerland, pp. 351, 352.
9. PERRET, W. R., *Ground Motion Studies at High Incident Overpressure*, The Sandia Corporation, Operation PLUMBBOB, WT-1405 for Defense Atomic Support Agency Field Command, June, 1960.